AECD-4226

General Electric Company
KNOLLS ATOMIC POWER LABORATORY
Schenectady, New York

SELF-SHIELDING MEASUREMENTS IN PPA-20

by

J. S. King

September 9, 1954

TABLE OF CONTENTS

LIST OF ILLUSTRATIONS

I INTRODUCTION

The self-shielding characteristics of a number of absorbers and of U-235 and U-238 have been investigated in PPA-20 (66°). Most of the measurements have been made in Ring 3 at the core mid-plane. The foil doubling technique was employed. Particular attention was given to "thin" foil regions for the purpose of extrapolating the data to zero thickness. In a few cases, namely Au, Ag, Cd and B, theoretical self-shielding curves have been calculated and found to be in good agreement with the experimental data. Both reactivity coefficient and activation experiments were undertaken for Au for the purpose of evaluating changes in F_L with self-shielding. In a number of cases the zero-width reactivity coefficient has been calculated and compared with the extrapolated data.

II SUMMARY OF RESULTS

The individual self-shielding curves for foils of Au, B, Cd, Ag, Ta, W, Hf, Rh, U-238, and fuel are shown in Figures 1 through 14. Extrapolation of the data indicates the following values for the zero-thickness reactivity coefficients (which we will henceforth denote by the initials R.C.).

TABLE I

ELEMENT	POSITION	R.C.($/mol)
Ag	R-3, Center	1.38 ± 7%
Au	" "	2.40 ± 5%
B	" "	0.89 ± 6%
Cd	" "	2.21 ± 6%
Cd	R-9 "	2.02 ± 6%
Hf	R-2 "	2.95 ± 10%
Rh	R-3 "	1.60 ± 20%
Ta	R-2 "	1.40 ± 8%
W	R-3 "	0.80 ± 15%
U-238	R-3 "	0.33 ± 20%

Comparison of these values with calculated thin foil R.C.'s is discussed in part IV.

R.C. measurements on wire samples of Cd, Ta, and W are shown in Figures 4, 8 and 9. These compare with the foil measurements as follows:

TABLE II

ELEMENT	R.C. ($/mol)	WIRE RADIUS	FOIL THICKNESS FOR SAME R.C.
Ta	0.534	0.0125"	0.013"
W	0.195	0.021"	0.021"
Cd	0.252	Rectangular Slivers 0.031" x 0.057"	0.018"

This is in good agreement with the approximate equivalence of width for slabs and radius for cylinders in the self-shielding calculations.

A comparison of the shape of all self-shielding curves that could be extrapolated to zero width is shown in Figure 14. This shows the individual shielding curves normalized to unity at zero width. A curve for Cd^{113} is also included. It was constructed from the natural cadmium curve assuming all the absorptions occur in Cd^{113}.

The variation in F_L with self-shielding was investigated by making simultaneous R.C. and activation measurements on Au foils. Since F_L connects the reactivity coefficient ($\frac{\Delta k}{k}$) with the absorption integral (Δa) according to the relation

$$\frac{\Delta k}{k} = \frac{F_L \cdot \Delta a}{\Sigma_f} \qquad (1)$$

a comparison of the R.C. and activation curves should reveal dependence of F_L on self-shielding. Figure 2 illustrates this comparison. It is evident that the variation, if it exists, over the range given is less than the experimental uncertainty of about 7%. Theoretical consideration of the effect is given in part IV.

III EXPERIMENTAL PROCEDURE

The standard measuring arrangement consisted in depressing all of the core slugs in R-3 (or R-2) of the stationary half about 5/8" away from the core interface and inserting the foil samples of standard PPA disk area in the cavities so provided. The thinnest samples were approximately 0.10 mils for Ag, Au, and Cd and 0.35 mils for Ta. In

order to obtain a sufficient reactivity change for these it was necessary to have the largest total foil area feasible. Ring 3 contains 12 slugs and provides a total foil area of 231.3 cm^2. This was found to be large enough to give changes of 1.1 to 2.0 cents for the thinnest samples. The uncertainty in PPA reactivity changes was about $\pm$ 0.08 cents so that the possible thin foil error was roughly 4.0 to 8.0% for a single measurement.

Solid metal foils were used throughout the measurements on Ag, Au, Cd, Rh, Ta and W. Insofar as possible, the practice was to make a run with all 12 slots of R-3 filled. Every other foil was then sandwiched together with its neighbor for a second run. Each succeeding run was made by doubling up on the remaining sandwiches. By this method the only change introduced was the thickness of the foils. Unfortunately, this could usually be done only for a thickness multiplication of 3 before more sample weight was needed to compensate for the reduction in reactivity with thickness.

The thinnest foil samples were mounted between 1.0 mil Al shields for handling purposes. Although the Al contributes negligibly to the reactivity change, zero runs were always made with an equivalent amount of Al in position. The uncertainty in the sample weights and uniformity for Ag, Au, Cd, and W is estimated to have less than 1% effect on the R.C. measurements. The Ta foils* were somewhat less uniform than the other materials. In all these cases, however, the uncertainties were small enough compared to the measurement errors to warrant their neglect. Also,

* Obtained from the G.E. Research Laboratory. The Ag, Au, Cd samples were obtained from the Baker Metals Co. of Newark, N. Y.

any small impurity effects were neglected in view of the fact that all cases examined were relatively strong absorbers.

Special samples of B and Hf were required. Natural boron was mixed with Al powder and cold pressed into 20.0 mil disks*. The data of Figure 3 was obtained with foil sets of two different B-Al mixtures, the first three thinnest points with one set and the two thicker points with the other. It appears that a small discontinuity occurs for the two sets indicating either a small error in the relative weights or an edge effect for the doubling of the thin set. Calibration checks of the two foil sets in the TTR indicate no significant weight error was involved. The possibility of an edge effect will be discussed below.

Metal foils were used for all but the two thinnest Hf points, as indicated on Figure 6. The latter points were obtained from samples of Hf O_2 + Al powder mixtures held in pancake type steel cans with an effective foil area of 15.047 cm^2 and a useful width of 0.218 cm. One mixture was chosen to give a point near the metal foil data so that the powder and foil data could be smoothly joined. A correction of 6.4% was applied to the powder data to accomplish this.

In all the measurements care was taken to provide an effective foil area to thickness ratio large enough to approach an infinite slab geometry. This precaution is most necessary in regions where the reactivity vs. thickness rate of change is maximum. If appreciable edge surface exists the volume to surface ratio is reduced and the effective foil thickness is smaller than the actual width. If the edge surface increases with foil

* The procedure previously developed by H. Hirsh of KAPL was used.

doubling the effect is to flatten the self-shielding curve when plotted as a function of actual width. The rule of thumb followed was to maintain the hydraulic radiub, r, which is defined by

$$r = \frac{2 \text{ volume}}{\text{surface}} \qquad (2)$$

to within 5% of the foil width x. This meant an upper limit of about 50 mils for x for the standard 0.97" radius, R, of PPA disks. Most samples were less than this, but the cases of B and Hf were exceptions. The upper 3 points of the B data in Figure 3 were obtained by sandwiches of 1, 2, and 4, 20 mil disks, the last sandwich therefore being 80.0 mils thick. The hydraulic radius for this sandwich is

$$r = \frac{x}{1 + \frac{x}{R}} = \frac{.080}{1 + \frac{.080}{.970}} = 0.0739"$$

or about 8% less than x. Reference to KAPL report 909, page 19 will show that the self shielding curves for the two asymptotic cases of an infinite slab and an infinite cylinder are nearly coincident when plotted against the hydraulic radius. Hence the curve for a finite cylinder (or thick disk) will lie between these limits. If the boron data were plotted against r rather than x the 20 mil sample point would not change significantly while the 80 mil point would be shifted to the left by 8% of the abscissa. Thus the edge correction required in Figure 3 would be to shift the point at 2.0×10^{-3} to 1.92×10^{-3} mols/cm^2. This is in the right direction but is much too small to account for the apparent displacement shown. It is indicated, therefore, that the displacement is more likely due to uncertainty in the critical measurement. In the case of the Hf O_2 samples, similar edge correction requires a displacement of about 10%. Here again the effect on the shape of the self-shielding

curve is negligible in view of the R. C. uncertainty.

The activation measurements on Au were made by irradiating 0.10 mil foils stacked in sandwiches of 1, 2, and 7 thicknesses. A fourth sample was made equivalent to a 40 foil sandwich by interspersing 7 0.10 mil foils between several 1.0 mil foils. The thin foils from each stack were removed from the pile and the 2.7 day β -activity recorded for each foil separately. The total activity of any stack was then found by adding the individual counts. For the thick stack, the thin foils served to sample the count rate at several depths so that a plot (Figure 15) of counts per foil versus thickness could be constructed and integrated numerically. This individual counting was done to eliminate systematic counting error due to β -absorption in Au samples of varying thickness. The total counting rates as a function of thickness were then converted to absorption rates by normalizing the data to a calibrated 2.3 mil Au foil activation.

IV THEORY & CALCULATIONS

A. General Self-Shielding Expression for Pure Absorbers

The calculation of absorption rates and reactivity coefficients in the presence of self-shielding is straightforward and much used. It is perhaps desirable to review the basic expressions here in order to display clearly the various assumptions used in calculating the self-shielding curves accompanying the present data. We will restrict ourselves to the case of a pure absorber in the form of an infinite slab.

As described by H. Hurwits in KAPL-98, the reactivity loss upon introducing an absorber in the pile is equal to the fractional loss in the total fission rate. This loss is equal to the number of neutrons removed from the pile per second times the probability they would have had for eventually producing fissions had the absorber not been present. Thus we write

$$\frac{\Delta k}{k} = \frac{1}{Z_f} \int_0^\infty F(E) \cdot n(E,t) \cdot dE \qquad (3)$$

where Z_f = total number of fissions per second per watt throughout the core

$F(E)$ = iterated fission probability of neutrons at the energy E, at the core position in question, and in the original, unpoisoned state.

$n(E,t)dE$ = number of neutrons in the energy interval dE throughout the absorber volume of total thickness t.

The number of neutrons in the interval dE absorbed per second is

$$n(E,t)dE = \sigma_a(E) \cdot N \left[\int d(\text{Vol}) \cdot \phi(E,x) \right] \cdot dE \qquad (4)$$

$$= \sigma_a(E)\, N \cdot 2A \left[\int_0^t dx\, \phi(E,x) \right] \cdot dE$$

where N = number of poison atoms/cm^3 of absorber

A = foil area

$\sigma_a(E)$ = atomic absorption cross section

$\phi(E,x)$ is the flux entering from one foil face which passes through unit foil area per second at a depth x from the face. In terms of the

flux at the outside of the foil it can be written in polar coordinates as

$$\phi(E,x) = \frac{\phi(E,0)}{2} \int_0^1 du \cdot e^{-N\sigma_T x/u} \tag{5}$$

where u is the cosine of the angle of incidence with respect to the normal to the foil face. σ_T is the total atomic reaction cross-section $\sigma_T = \sigma_s + \sigma_a$. Equation (4) then becomes

$$\begin{aligned} R(E,t)dE &= (NA)\sigma_a(E)\phi(E,0)\left[\int_0^t dx \int_0^1 du \cdot e^{-N\sigma_T x/u}\right] dE \\ &= (NAt)\sigma_a(E)\phi(E,0)\left[\int_0^1 \frac{du}{u}\left(\frac{1-e^{-N\sigma_T t/u}}{N\sigma_T t}\right)\right] \cdot dE \end{aligned} \tag{6}$$

Using the substitutions $N\sigma_T t = S$, which is a function of energy through σ_T, we let

$$\begin{aligned} f(S) &= \frac{1}{S}\int_0^1 (1-e^{-S/u})\frac{du}{u} \\ &= \frac{1}{2S}\left\{1-e^{-S}+Se^{-S}-S^2\int_S^\infty \frac{e^{-y}}{y}dy\right\} \end{aligned} \tag{7}$$

Then using (7) in (6) and (6) in (3) we have

$$\frac{\Delta k}{k} = -\frac{(NAt)}{\Sigma_f}\int_0^\infty dE\,\sigma_a(E)\,\phi(E,0)\,F(E)\cdot f(S) \tag{8}$$

(NAt) is the number of poison atoms introduced. If we set this equal to Avogadro's number (A.N.) and multiply both by $\frac{1}{\beta}$ *, we have the reactivity loss in dollars per mol of absorber of thickness t:

$$\frac{\Delta k}{k}\left(\frac{g}{Mol},t\right) = \frac{-A.N.}{\Sigma_f \beta}\int_0^\infty dE \cdot \sigma_a(E)\,\phi(E,0)\,F(E)\,f(S) \tag{9}$$

* β is the effective delayed neutron fraction

In the limit of very thin foils $\delta \to 0$ and $f(\delta) \to 1.0$ so that we may define an effective self-shielding factor

$$\mathcal{F}(t) = \frac{\int_0^\infty dE\, \sigma_a(E) \cdot \phi(E,0)\, F(E)\, f(\delta)}{\int_0^\infty dE\, \sigma_a(E)\, \phi(E,0)\, F(E)} \qquad (10)$$

We can also define an effective F_L which is in principle a function of t through $f(\delta)$

$$F_L(t) = \frac{\int_0^\infty dE \cdot \sigma_a(E) \cdot \phi(E,0)\, F(E)\, f(\delta)}{\int_0^\infty dE\, \sigma_a(E)\, \phi(E,0)\, f(\delta)} \qquad (11)$$

and an absorption integral which is also a function of t

$$\Delta a(t) = \int_0^\infty dE\, \sigma_a(E)\, \phi(E,0)\, f(\delta) \qquad (12)$$

This allows us to rewrite (9) as

$$\frac{\Delta k}{k}(t) = -\frac{A \cdot N}{\xi_f \beta} \cdot F_L(t) \cdot \Delta a(t) \qquad (13)$$

Finally, we can express the effective self-shielding factor in terms of measurable reactivity ratios or absorption and F_L ratios:

$$\mathcal{F}(t) = \frac{\left(\frac{\Delta k}{k}\right)(t)}{\frac{\Delta k}{k}(0)} = \frac{F_L(t) \cdot \Delta a(t)}{F_L(0)\, \Delta a(0)} \qquad (14)$$

B. <u>Special Case of Single Resonance Absorbers</u>

If the total absorption of a nuclide is due mainly to a single resonance which obeys a Breit-Wigner formula

$$\sigma_a(E) = \frac{\sigma_a(E_0)\, \left(\frac{E_0}{E}\right)^{1/2}}{1 + \left(\frac{E - E_0}{\Gamma/2}\right)^2} \qquad (15)$$

and if $E_0 \gg \Gamma$ formulas (9) through (12) are simplified because the approximations that $\phi(E)$ and $F(E)$ are constant over the important region of absorption are very good. These factors can be removed from the integrals with the result that

$$\frac{\Delta k}{k}(t) \approx -\frac{\Delta N}{\bar{\nu}\beta} \cdot F(E_0) \cdot \phi(E_0) \cdot \int_0^\infty dE \cdot \sigma_a(E)\, f(\delta) \qquad (9\text{-a})$$

$$\mathcal{F}(t) \approx \frac{\int_0^\infty dE \cdot \sigma_a(E) \cdot f(\delta)}{\int_0^\infty dE\, \sigma_a(E)} \qquad (10\text{-a})$$

$$F_2(t) \approx F(E_0) \qquad (11\text{-a})$$

$$\Delta a(t) \approx \phi(E_0) \int_0^\infty dE \cdot \sigma_a(E) \cdot f(\delta) \qquad (12\text{-a})$$

These relations illustrate several interesting properties of absorbers with a predominant single resonance:

(1) From (10-a) it is seen that the self-shielding characteristic is just the self-shielding factor $f(\delta)$ averaged over a Breit-Wigner resonance peak. It is independent of the flux. $\mathcal{F}(t)$ or rather the more universal function $\mathcal{F}(\xi_0)$, where

$$\xi_0 = N\sigma_t(E_0)\, t$$

has been calculated by G. H. Roe for a single resonance with and without Doppler corrections applied to the resonance parameters.* Figure 16 is a reproduction of $\mathcal{F}(\xi_0)$ vs ξ_0 for zero temperature** (i.e. no Doppler correction). Also plotted is the universal function $f(\xi_0)$ as obtained from (7).

* KAPL MEMO-GHR-4

** Doppler corrections are unimportant for most of the data herein presented.

(2) Equation (11-a) indicates that $F_L(t)$ is just the value of $F(E)$ at E_0 and is independent of the degree of self-shielding for a single sharp resonance.

(3) Experimental measurements of $\frac{\Delta k}{k}(t)$ carried to values of t small enough to allow an extrapolated estimate of $\frac{\Delta k}{k}(t = 0)$ can be used to measure the resonance level strength $(\sigma_a(E_0)\cdot\Gamma)$. In the limit of $\zeta_0 << 1.0$ $f(\zeta) \approx 1.0$ and (12-a) together with (15) give

$$\Delta\alpha(t=0) = \phi(E_0)\int_0^\infty dE\cdot\sigma_a(E)$$

$$\approx \phi(E_0)\cdot\sigma_a(E_0)\int_0^\infty \frac{dE}{1+\left(\frac{E-E_0}{\Gamma/2}\right)^2}$$

$$= \phi(E_0)\cdot\frac{\pi}{2}\left[\sigma_a(E_0)\cdot\Gamma\right] \qquad (12\text{-}6)$$

and hence

$$\frac{\Delta k}{k}(t=0) = -A\cdot N\cdot\frac{\phi(E_0)}{\Sigma_f}\cdot\frac{F(E_0)}{\beta}\cdot\frac{\pi}{2}\left[\sigma_a(E_0)\cdot\Gamma\right] \qquad (9\text{-}6)$$

$F(E_0)$ is believed to be an insensitive function of energy. It may be evaluated for a particular energy region by measuring $\frac{\Delta k}{k}(t = 0)$ and $\phi(E_0)$ for a resonance absorber with known $(\sigma_a(E_0)\cdot\Gamma)$. If the variation of $\phi(E)$ is known (9-6) can then be used to find the level strength of any other sample whose absorption is due to a resonance in this region.

(4) In principle, extension of the shielding data in the opposite extreme of thick foils ($\xi \gg 1.0$) provides an independent measure of the product $\sigma(\epsilon_i)\Gamma^2$ and hence with the results of part (3) a determination of $\sigma_a(\epsilon_i)$ and Γ separately. However, it occurs even for a strongly mono-resonance absorber like Au, that absorption by subsidiary peaks (and the 1/v component) become predominant in the thick foil region. This obscures the main resonance characteristic and prevents a good measurement of $\sigma_a(\epsilon_i)\Gamma^2$.

C. Multiple-Resonance Absorbers

Except for a few abnormal cases such as cadmium, most heavy nuclides exhibit not one but many absorption and scattering resonances in the epi-cadmium region, with an average level spacing of the order of 5 to 100 e.v.* The result of multiple resonance is to flatten the overall self-shielding curve by raising the thick foil region ($\xi_0 > 1$). Assuming that the level spacing is large enough so that overlapping of the "wings" of adjacent resonances is negligible, the total absorption and reactivity can be written as the sum of individual contributions as given by (9-a) and (12-a) above. We can rewrite these expressions as

$$\frac{\Delta K}{K}(t) = \frac{-AN}{\xi\beta}\sum_j F(\epsilon_j)\cdot\Delta a_j(t) \qquad (16)$$

where E_j is the resonant energy of the jth peak. Using equations (14) and (12-b) this gives

* J. M. Blatt and V. F. Weisskopf, Theoretical Nuclear Phy... (John Wiley and Sons, 1952), p. 475

$$\frac{\Delta k}{k}(t) = \frac{-A N_i}{\Sigma_f \beta} \sum_j F(\xi_j)\cdot \Delta a_j(a)\cdot \mathcal{F}(\xi_j)$$

$$= \frac{-A N_i}{\Sigma_f \beta}\cdot \frac{\Pi}{2} \sum_j \left(F(\xi_j)\,\phi(\xi_j)\,\sigma_a(\xi_j)\,\Gamma_j\right)\cdot \mathcal{F}(\xi_j) \qquad (17)$$

where we write the general notation $\mathcal{F}(\xi_j)$, $\xi_j = N\sigma(\xi_j)t$ since now the peak cross section varies from resonance to resonance. It is to be noted that for a particular t, $\mathcal{F}(\xi_j)$ depends only on the relative amplitude of the peak cross section $\sigma_a(\xi_j)$. In the simplest case of an absorber with just two resonances of equal amplitude, $\mathcal{F}(\xi_j)$ is constant with j and is removed from the summation in (17). The result is a self-shielding curve identical in shape with the single-resonant curve but of different amplitude. If, however, $\sigma(\xi_j)$ is small for one of the peaks relative to the other, the value of $\mathcal{F}(\xi_j)$ at a particular t for the large peak will be taken from Figure 16 at a larger ξ than for the small one. Equation (17) then gives the sum of two curves each identical with Figure 16 but displaced from each other and with different amplitudes. A t which is "thick" for the large peak will be "thin" for the small peak and the effect is to prevent the overall shielding characteristic from falling as rapidly as in Figure 16.

All of the curves investigated herein exhibit this effect in varying degrees. The gold data (Figure 2) illustrates the case for an absorber with one large resonance and an undetermined number of much smaller resonances. The dashed curve is $\mathcal{F}(\xi)$ for the parameters appropriate to the giant peak at 4.9 e.v. The

solid curve is the sum of this $\mathcal{F}(\xi)$ and an additional constant term equal to 10% of the total R. C. evaluated at zero thickness*. This extra term represents the extra-resonance component of absorption, composed of peaks assumed small enough so that over the range shown their self-shielding could be neglected. It is seen that the data fits this composite curve exceedingly well except perhaps at the thickest point where self-shielding of the subsidiary peaks undoubtedly becomes significant.

In principle any multi-resonance case can be calculated according to equation (17) if Γ_γ, ϕ, and the level strengths are known. The real difficulty, however, is our current lack of knowledge of the resonance cross sections and level densities of practically all nuclides in the energy range above about 50 ev. The problem is well illustrated in the case of silver. The solid curve of Figure 1 was calculated according to equation (17). The level strength data used, which is obviously quite limited in energy range, is shown in Table III. It was taken from recent Brookhaven fast chopper results.** The flux spectrum used is shown in Figure 17 as measured in PPA-20. It was assumed that Γ_L was constant over the energy range involved and $\frac{\Gamma_\gamma}{\beta} = \$129$.

---

* This percentage was experimentally determined by the triple foil activation technique. See for example, KAPL 329, part I, p. 21

** In this report Γ_γ is assumed constant = 0.13 e.v. for all levels except the low energy resonance at 5.22 e.v. where it was measured to be 0.156 e.v.

TABLE III

Isotope	% Abundance	E_0	$\alpha\Gamma^2$ (b-ev^2)	$g\Gamma_n$ (mv)	$\phi(E_0)$/mm Hg/ev
Ag-107	51.4	16.6	60 ± 7	5.6 ± 0.8	.042 x 10^6
		42.4	45 ± 15	10 ± 4	.021
		45.6	8 ± 2	2.1 ± 0.6	.019
		52.2	150 ± 30	36 ± 10	.017
Ag-109	48.6	5.22	775 ± 25	12.2 ± 0.5	.102
		31.1	52 ± 6	9.0 ± .2	.025
		40.8	34 ± 10	8 ± 3	.021
		56.8	95 ± 25	24 ± 6	.016
		72.5	150 ± 30	47 ± 15	.013
		88.5	21 ± 5	10 ± 3	.011

The discrepancy between calculated and experimental curves can be described as follows:

(1) The absolute magnitude of the calculated curve at zero thickness is \$1.05 as against a measured R. C. of \$1.38 ± 7%. The calculation does not include the 1/v absorption component. From the thermal cross sections of boron and silver and the experimental thin-foil R. C. for boron, a reliable estimate for this component is \$0.07. This brings the calculation to \$1.12. The remaining difference of \$0.26 ± 0.00 suggests that there are a number of resonances unaccounted for.

(2) A normalization of the calculated curve of Figure 1 to fit the data at zero thickness is still a poor fit at large foil thicknesses. This indicates that the peaks are on the average much smaller than the giant 5.22 ev resonance because they must have relatively small self-shielding factors.

(3) A precise fit with the data can be obtained by adding a number of peaks with self-shielding factors similar to the small peak at 40.8 ev in Table III. This is shown by the solid curve in Figure 1-a which was obtained by adding enough of these peaks to the Table III group to give the correct R. C. at zero thickness. The Brookhaven authors are confident that no peaks of this order of amplitude (for $\ell = 0$) are unaccounted for below 100 ev. The conclusion is, therefore, that the above reactivity discrepancy, about 20% of the total absorption, is due to unresolved resonances above 100 ev.

D. Cadmium and Boron

These two elements constitute exceptions to the general classification of multi-resonance materials studied. Figure 4 shows two calculated curves for Cd. The dashed curve is $\mathcal{P}(\xi)$ for the parameters shown. The solid curve is a numerical integration according to equation (9) using cross-section data from AECU-2040 and the spectrum given by the curve in Figure 17. Although Cd is essentially a singly resonant element,

the self-shielding characteristic was not expected to be accurately given by $\mathcal{F}(\xi_o)$ since it is in a region where E_o is not large compared to Γ ; the large thermal tail and more or less flat spectrum combine to give a shape more closely resembling $f(\xi_o)$ than $\mathcal{F}(\xi)$. The solid curve of Figure 5 is the same curve as used in Figure 4, normalized to the lower R. C. value at the core edge (this was done for lack of spectrum measurements in Ring 9). The extremely good fit to the data would indicate that differences in the spectrum shape are not very important, however, over the region of large cadmium absorption. The poorer fit in Figure 4 for thicknesses greater than about 2.10^{-3} mols/cm^2 suggests that there is a significant contribution to the absorption from higher energy reactions (the numerical integration was carried to 1.0 ev). The spectrum above 1.0 would be expected to fall off heavily relative to that below 1.0 ev in going from the core center to the core edge and this would explain the lack of a similar misfit for the core edge data of Figure 5. Except for this thick region, however, the experimental curves compare very closely.

The solid curve for natural boron in Figure 3 was found by a straight integration of equation (9) using again known cross section and flux data as for cadmium. A constant value was used for F(E) or $F_L(E)$ and this probably introduces a certain error at high energies. The flux curve above 300 volts was assumed to be a straight-line extrapolation of Figure 17. The measurements are limited enough so that the effects of these assumptions cannot be evaluated.

E. Variation of F_L of Gold with Foil Thickness

It was proposed in part B that for the idealized case of a single resonance absorber $F_L(E)$ as given in equation (11) degenerated to (11-a)

and was approximately the value of F (E) at E_0, independent of self-shielding. In reality this is only true up to the thickness where the wings of the resonance or other extra-resonance components of the absorption cross-section begin to constitute an appreciable fraction of the total absorption rate. The effect of self-shielding on equation (11) is to give increasing weight to the values of F (E) in the extra-resonance energy regions (or in the case of multi-resonance absorbers at the resonant energies of the minor peaks).

For gold some 87% of the total absorption at zero thickness was due to the neutron flux between 4.0 and 6.0 ev. However, this dropped to only 12% of the total absorption at a thickness of 50.0 mils. In the latter case roughly 48% was due to neutron flux above 6.0 ev (absorption in an unknown number of higher energy resonances) and 40% to flux below 4.0 ev (absorption in the large thermal tail of the main resonance). Hence, if F (E) decreased in a monotonic manner with an increase in energy, it might be expected that the thick foil F_L could be very close to the zero thickness F_L; the larger average F (E) in the low energy region and the smaller average F (E) in the high energy region compensate each other and give an overall average for the thick foil in agreement with the F (E) at 4.89 ev. As noted above, the experimental variation in F_L up to 40 mils was at least less than the experimental uncertainty of about ± 7%, in accordance with our expectation of little or no change.

Recent multigroup calculations for a core approximating PPA-20 have provided the flux self-adjoint function at the core center[4].

[4] From unpublished data supplied by P. Hofmann of KAPL

Figure 13 shows F(E) vs E obtained by normalizing the adjoint curve to an F(E) of 1.10 at 4.9/ev. Calculations of the variation of F_L for Au, based on this curve together with the spectrum of Figure 17 and gold cross-section data, result in a ratio of F_L for a 50 mil foil to F_L at zero thickness of between 1.015 and 0.980. The limits are set by the uncertainty in the choice of an average F(E) in the high energy region since there the Au cross-section is not known. It is evident, however, that the calculations are entirely consistent with experiment and indicate that the F_L variation is less than 2%.

F. Evaluation of Resonance Parameters from R. C. Data Near Zero Thickness

In addition to revealing the nature of reactor materials at high dilution, an experimental determination of unshielded R. C's. in an intermediate energy spectrum may provide considerable knowledge about average resonance structures in the energy region above 100 volts or so - a region not yet resolved by neutron spectroscopists.

If equation (17) is evaluated when $t \to 0$, then $\mathcal{F}(\xi_j) \to 1.0$ for all j and the summation is greatly facilitated since it is now simply the sum of level strengths weighted by F (E) and ϕ (E). The peak cross-sections $\sigma(\epsilon_j)$ can be written in terms of the level widths

$$\sigma(\epsilon_j) = 4\pi \lambda_j^2 g \left(\frac{\Gamma_n \Gamma_\gamma}{\Gamma^2}\right)_j = \frac{\hbar^2}{2\pi m} g \cdot \left(\frac{\Gamma_n \Gamma_\gamma}{\Gamma^2}\right)_j \cdot \frac{1}{E_j} \qquad (18)$$

Equation (17) now reduces to*

$$\frac{\Delta K}{K}(t \to 0) = C \sum_{j=0}^{\infty} \left(\frac{2g \Gamma_n \Gamma_\gamma}{\Gamma_n + \Gamma_\gamma}\right)_j \cdot \frac{1}{E_j} \cdot F_L(\epsilon_j) \cdot \phi(\epsilon_j) \qquad (19)$$

where $$C = \frac{(A+1)^2}{\Sigma_f \beta} \cdot \frac{\hbar^2}{\delta}$$

* The actual measured R.C. will contain an additional 1/v absorption component as noted above.

According to the theoretical interpretations of Weisskopf and others* it is commonly assumed that the average level spacing $\bar{D}$**, and the radiation width, Γ_γ, are more or less independent of the energy in the kilovolt region. Further, it is assumed that Γ_n is proportional to the square root of the resonant energy. Accordingly, the following conditions are assumed:

$$\begin{aligned} \Gamma_{nj} &= \Gamma_n^\circ E_j^{1/2} \\ \Gamma_{\gamma j} &= \Gamma_\gamma \\ E_j &= E_0 + j\bar{D} \approx \bar{D}(1+j) \end{aligned} \qquad (20)$$

Γ_n° is the "reduced" neutron width at 1.0) ev. E_0 is the energy of the first resonance and is expected to be roughly equal to $\bar{D}$. Equation (19) now can be written as

$$\frac{\Delta K}{K}(t\to\infty) = C \cdot 2g\,\Gamma_n^\circ \sum_{j=0}^{\infty} \left(\frac{1}{\frac{\Gamma_n^\circ}{\Gamma_\gamma} E_j + E_j^{1/2}} \right) \cdot F_L(E_j) \cdot \phi(E_j) \qquad (21)$$

Further simplification results if F_L and ϕ can be well represented by a power of the energy:

$$\begin{aligned} F_L(E_j) &\approx F_L(1.0)\, E_j^{-\alpha} \\ \phi(E_j) &\approx \phi(1.0)\, E_j^{-\beta} \end{aligned} \qquad (22)$$

These relations are quite reliable for the core center of PPA-20 between 10 ev. and about 10 kv. From the spectrum of Figure 17 β is about 0.76. α is extremely small. Multigroup calculations indicate a value of 0.014 over the above energy interval. We therefore write

* Blatt & Weisskopf, op. cit, p. 390

** The $\bar{D}$ here used is half the D referred to in the literature as the distance between levels of the compound nucleus with the same spin J. Assuming only $\ell = 0$ neutron reactions J has only two values $I \pm 1/2$ where I is the total spin of the target. Hence the distance between any two adjacent levels regardless of J should on the average be half the usual D.

$$\frac{\Delta k}{k}(t\to 0) = C' \cdot 2g\,\Gamma_n^0 \sum_{j=0}^{\infty} \frac{1}{E^{k+\alpha+\beta}\left(1+\frac{\Gamma_n^0}{\Gamma_j}E_j t\right)} \qquad (23)$$

where $$C' = C\, F_L(1.0)\, \phi(1.0)$$

Changing the variable of summation by letting $\Theta = (1+j)$, $E_j \approx \bar{D}(1+j) = \bar{D}\Theta$ and (23) becomes finally

$$\frac{\Delta k}{k}(t\to 0) = C' \left(\frac{2g\,\Gamma_n^0}{\bar{D}^k}\right) \sum_{\Theta=1}^{\infty} \frac{1}{\Theta^b(1+a\Theta t)} \qquad (24)$$

where $$b = k+\alpha+\beta$$
$$a = \left(\Gamma_n^0 \cdot \bar{D}^{k}/\Gamma_j\right)$$

It is assumed that the sum converges rapidly enough so that there is no significant difference between an upper limit at ∞ or at 10 kv or more.

In general, the sum cannot be reliably used below about 100 ev. This is because there are deviations in D and Γ_n^0 for individual levels - it is only the average over many levels that can be expected to have meaning. These deviations strongly effect the total R. C. if they occur at energies below 50 ev or so where the peak σ and the flux are very large. The isolated giant resonances in Au, Ag, Rh, etc. below 10 ev can be considered extreme examples; a strict use of (24) (i.e. starting the sum at $\Theta = 1$) would underestimate these giant resonances and produce large errors.

The practical way to use equation (24) is as a supplement to known (measured) resonance structure below 100 or 200 ev. That is, the reactivity contributions from individual known resonances are calculated in the region where spectroscopists can and have resolved the level strengths. The sum in equation (24) is then made starting

at the top of this region. The high energy component should then be obtainable using the average parameters measured in the low region. Conversely, the sum may be used to test the validity of these parameters at larger energies. The larger the fraction of $\frac{\Delta K}{K}$ belonging to this region the more sensitive is the test.

An example may be made of the silver data. As noted above the calculated sum of level strengths from data reported up to 100 ev leaves some 20% of the measured R. C. still unaccounted for. Using the pile characteristics quoted above (α and β) together with the reported silver parameters

Ag^{107} $\quad \Gamma_n^0 = 0.0021$ ev
$\quad D = \frac{50}{2} = 25$ ev

Ag^{109} $\quad \Gamma_n^0 = 0.0030$ ev
$\quad D = \frac{33}{2} = 16.5$ ev

the contribution from absorptions above 100 ev is calculated from equation (24) starting with the first 0 above 100 ev. It is found to be \$0.12 ± .02. The amount required by R. C. measurement is \$0.26 ± 0.07.

A second example calculated is Ta^{181}. The published data on observed resonances are given in Table IV. These data

TABLE IV

Isotope	% Abundance	E_0	$\sigma_0 \Gamma^2$ (b-ev^2)	$2g\Gamma_n$ (mv)	$2g\Gamma_n^0$ (mv)
Ta-181	100%	4.29 ± .02	59 ± 5	1.9	0.9
		10.36 ± .05	32 ± 5	2.5	0.8
		13.9 ± 0.1	12 ± 2	1.3	0.3
		20.7 ± 0.2	7 ± 2	1.1	0.2
		24.2 ± 0.2	27 ± 5	5.0	1.0
		36.7 ± 0.3	250	71.0	11.7
		39.4 ± 0.5	180	54.0	8.6

were obtained with the Brookhaven crystal spectrometer.* The neutron widths were found by assuming a constant Γ = 0.102 ev. The widths are not appreciably different from the Columbia velocity spectrometer result.** In the latter case a constant Γ (0.100 ev) was also assumed.

The calculation gives $0.72 for the region 0.0 to 50.0 ev, $0.63 for the region above 50.0 ev, and $0.02 for the 1/v component, which is a total of $1.37. The measured R. C. for thin tantalum was $1.40 ± 8%.

A third example is natural hafnium. Data on the isotopes Hf - 177, 178, 179 and 180 between 0.0 and 100.0 ev is given in Table V, as reported by the Brookhaven velocity spectrometer group.***

---

* Christensen, R. L., "Slow Neutron Resonances in Tantalum. P. R. vol. 92 p, 1509 (1953)

** Melkonian, E., Havens, W. W. Jr., and Rainwater, L. J., "Slow Neutron Velocity Spectrometer Studies. V. Re, Ta, Ru, Cr, Ga" P. R. Vol. 92 p, 702 (1953)

*** Private communication between J. Harvey of Brookhaven and N. Yeater of KAPL

Isotope	% Abundance	E_o	$g_n \Gamma^2$ (b-ev^2)	$2g\Gamma_n$ (mv)	$2g\Gamma_n^o$ (mv)	$\Gamma = \Gamma_n + \Gamma_\gamma$	Remarks
Hf-177	18.4%	1.08	110	2.0	1.92	45	
		2.3	280	4.5	2.97	83	
		5.9	80	5.5	2.27	60	Γ = 60 mv assumed
		6.5	170	11	4.31	60	
		9.0	41	3.5	1.17	80	Γ = 80 mv assumed
		14.1	42	4	1.06	120	
		22.5	17	2.4	.51	102	Γ_γ = 100 mv assumed
		23.6	3.9	.7	.14	102	" " "
		27.3	7.6	1.6	.31	102	" " "
		33.2	5.3	1.3	.23	101	" " "
		37.0	46	11	1.80	111	" " "
		46.8	62	18	2.66	118	" " "
		49.1	220	53	7.58	153	" " "
		56.0	63	22	2.95	122	" " "
		57.2	20	8.4	1.11	108	" " "
		64.6	140	46	5.70	146	" " "
		68.4	91	36	4.36	136	" " "
		71.3	14	7.1	.84	107	" " "
		75	38	18	2.07	118	" " "
		85.8	12	7.2	.78	107	" " "
		87.4	15	8.9	.95	109	" " "
		94.4	12	7.7	.79	108	" " "
		100.1	32	20	2.00	120	" " "
Hf-178	27.1%	7.8	1500	50	17.9	88	" " "
Hf-179	13.8%	5.7	70	4.5	1.89	60	Γ = 60 mv assumed
		17.7	11	1.4	.33	101	Γ_γ = 100 mv assumed
		23.9	29	46	9.43	105	" " "
		26.5	5.6	1.0	.19	101	" " "
		31.5	18	3.9	.69	104	" " "
		36.9	75	18	2.97	118	" " "
		40.5	80	21	3.30	121	" " "
		42.6	26	7.5	1.15	108	" " "
		69.7	16	8.0	.96	108	" " "
Hf-180	35.3%	74.0	200	35	4.06	165	" " "

The reactivity coefficient for natural hafnium has been calculated from these data under the assumption that Hf-174 and 176 have no significant effect. The total contribution for the 1/v component is \$0.12, for the 0-100 ev region \$2.07, and for the region above 100 ev \$0.12. This gives a total of \$2.30 as compared to a measured value of \$2.95 ± 10%.

The calculations and measurements are summarized in Table VI for hafnium, silver and tantalum.

TABLE VI

Isotope	% Nat. Ab	$2g\Gamma_n^0$ (mv)	D (ev)	$\left(\frac{2g\Gamma_n^0}{D}\right)_{n/D^+}$	Calculated RC ($/mol) 1/v	0-100	100-∞	Tot	RC of Nat. Element ($/mol) Calc.	Observed
Ag-107	51.4%	2.1	25.0	0.84	0.04	0.24	0.08	0.36	1.25	1.38 ± 5%
Ag-109	48.6%	3.0	16.5	1.82	0.11	1.91	0.17	2.19		
Ta-181	100%	3.4	6.0	5.6	0.02	0.72 (0-50ev)	0.63 (50-00)	1.37	1.37	1.40 ± 8%
Hf-177	18.4%	2.11	4.35	4.85	0.38	7.42	0.49	8.29		
Hf-178	27.1%	17.8	~100	1.78	0.11	2.24	~0.01	2.36	2.30	2.95 ± 10%
Hf-179	13.8%	2.32	11.1	2.09	0.08	0.58	0.19	0.85		
Hf-180	35.3%	4.07	~100	0.41	0.02	0.05	~0.0	0.07		

Several general conclusions about these calculations are in order, even though the number of cases investigated here is too small for any statistical evaluation:

(1) It is possible that the total R.C. calculations generally tend to be lower than experiment. Table VI shows that the calculations account for 91% of the observed R.C., for Ag, 98% for Ta, and 78% for Hf. The close agreement for Ta may be fortuitous for it is suspected that the average reduced neutron width is unrealistically large as a result of the two abnormal levels at 35.1 and 38.2 ev.

(2) If this tendency is real the explanation is either that

(a) The average resonance parameters used in the high-energy sum (equation (24) for θ above $\frac{100}{D}$) above the resolved region are incorrect, or

(b) The resonance structures reported in the literature for the low energy (resolved) region are incomplete (this presumable could occur if a number of small resonances exist in the region below 100 ev too small to be resolved by present spectroscopic technique), or

(c) The assumptions in equations (20) for the energy dependence of Γ_γ , Γ_n, and D are not valid.

(3) If alternative (b) is correct practically all of the calculation error could be assigned to the low energy region. This would presumably require a large change in the choice of $2g\Gamma_n^\circ$ and $\bar{D}$ but not necessarily in the ratio $\frac{2g\Gamma_n^\circ}{\bar{D}}$ (which ratio most sensitively affects the calculated high-energy sum).

(4) If alternative (a) is correct, a rather drastic correction in the ratio $\frac{2g\Gamma_n^\circ}{\bar{D}}$ is required in the present cases of Ag and Hf because we would now assign all the discrepancies to the small fraction of the R.C. due to absorptions above 100 ev. Table VI shows that if we assume no error in the 1/v and 0-100 ev calculations the 100 - ∞ ev sums account

for only a fraction of the absorptions required for agreement between calculation and experiment for the total R.C.'s - 45% for Ag, 91% for Ta, and 16% for Hf.

In any event investigation of many more multi-resonance cases is needed to establish any general trend. Also, it is clear that the accuracy of the measured R.C.'s must be improved to the point where the uncertainty in the R. C. is small compared to the high-energy calculated component. Further experimental work toward this end is planned.

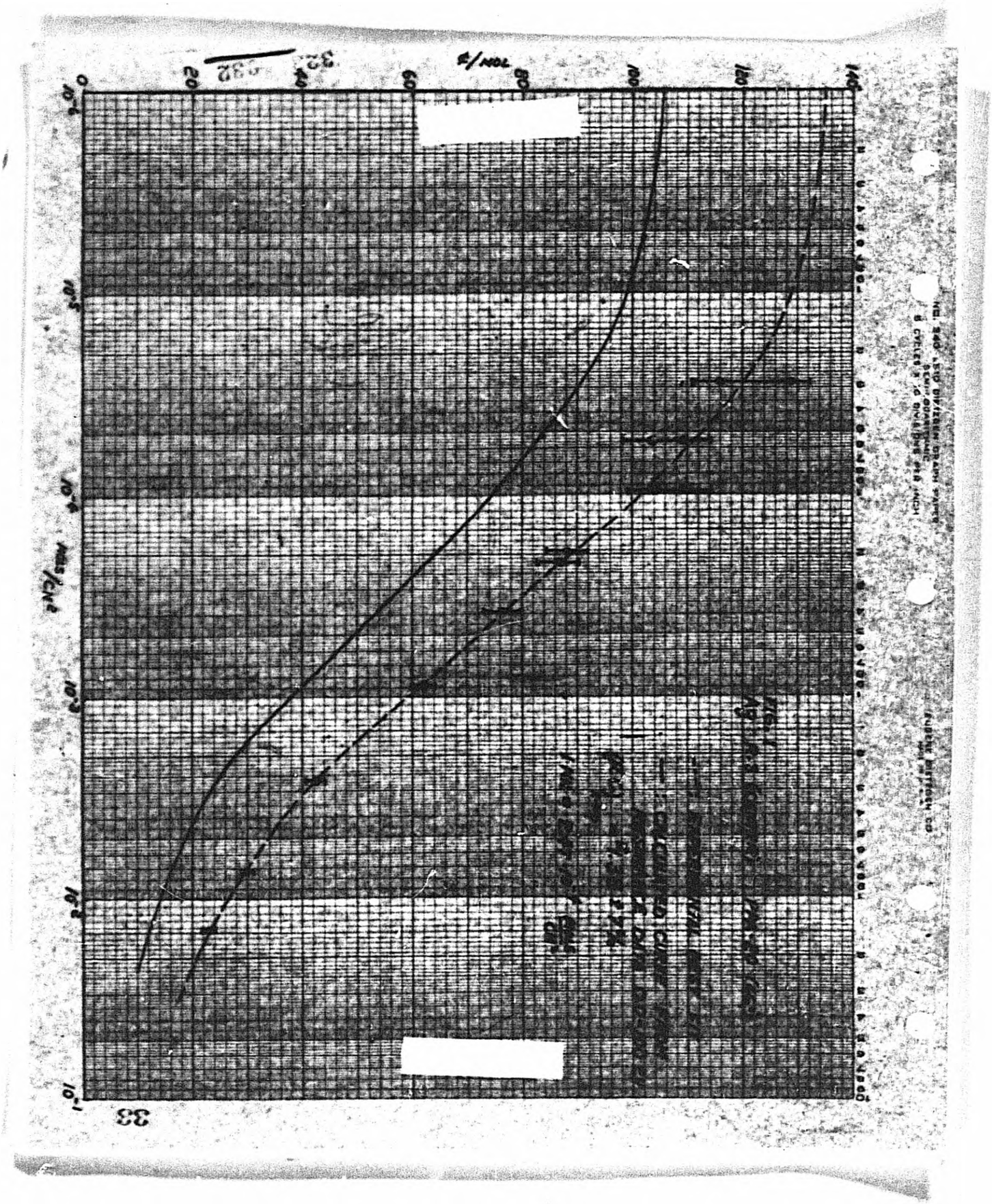
TON/ft
0
20
40
60
80
100
120
140
10^{-2}
10^{-1}
10^{0}
10^{1}
10^{2}
10^{3}
LBS/IN²
33

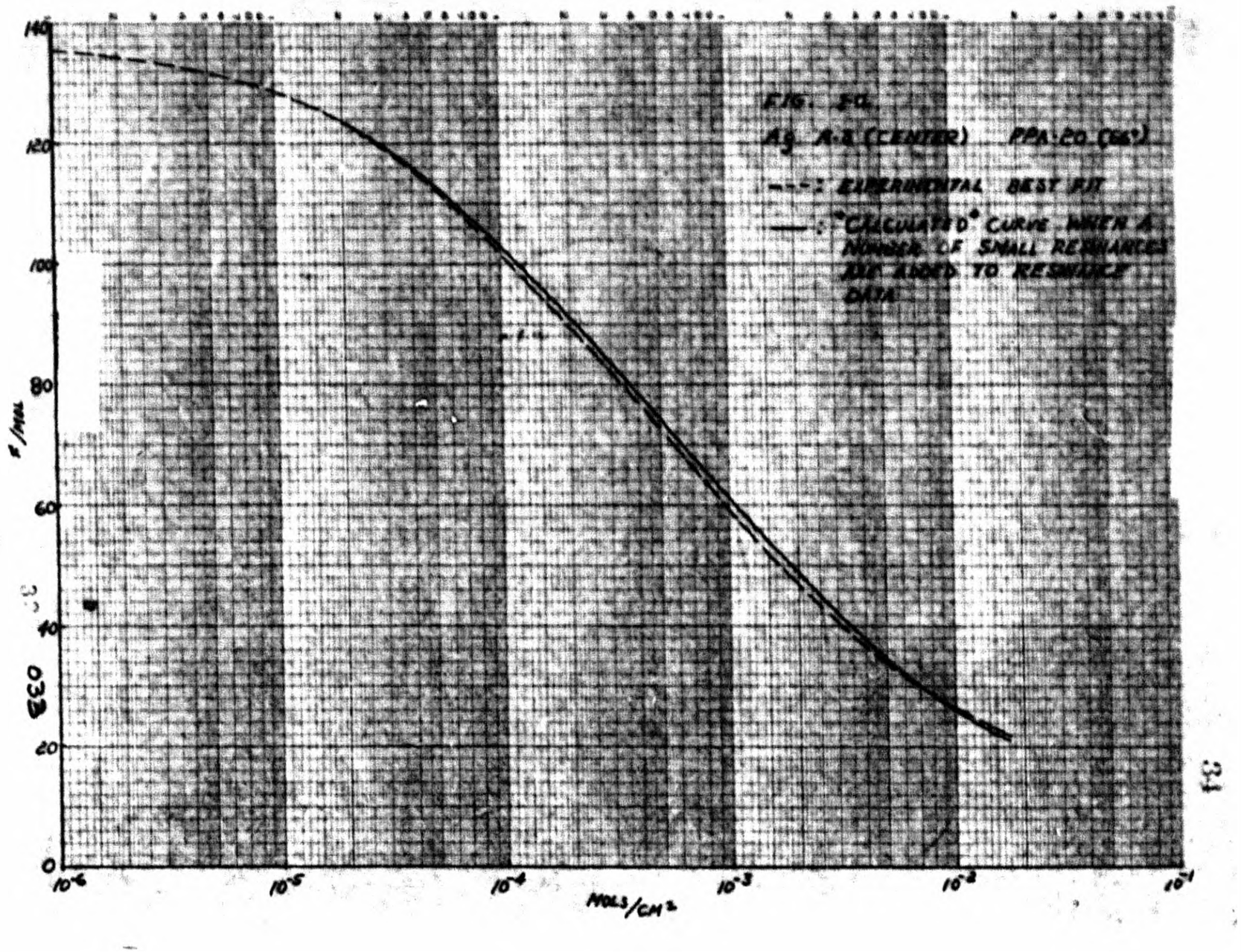
FIG. 5C.
Ag A-2 (CENTER) PPA: 20 (Sat)
---: EXPERIMENTAL BEST FIT
——: "CALCULATED" CURVE WHEN A NUMBER OF SMALL REINFORCES ARE ADDED TO RESIDUE DATA
140
120
100
80
60
40
20
0
F/MM
ESO
10^{-6}
10^{-5}
10^{-4}
10^{-3}
10^{-2}
10^{-1}
MOLS/CM²

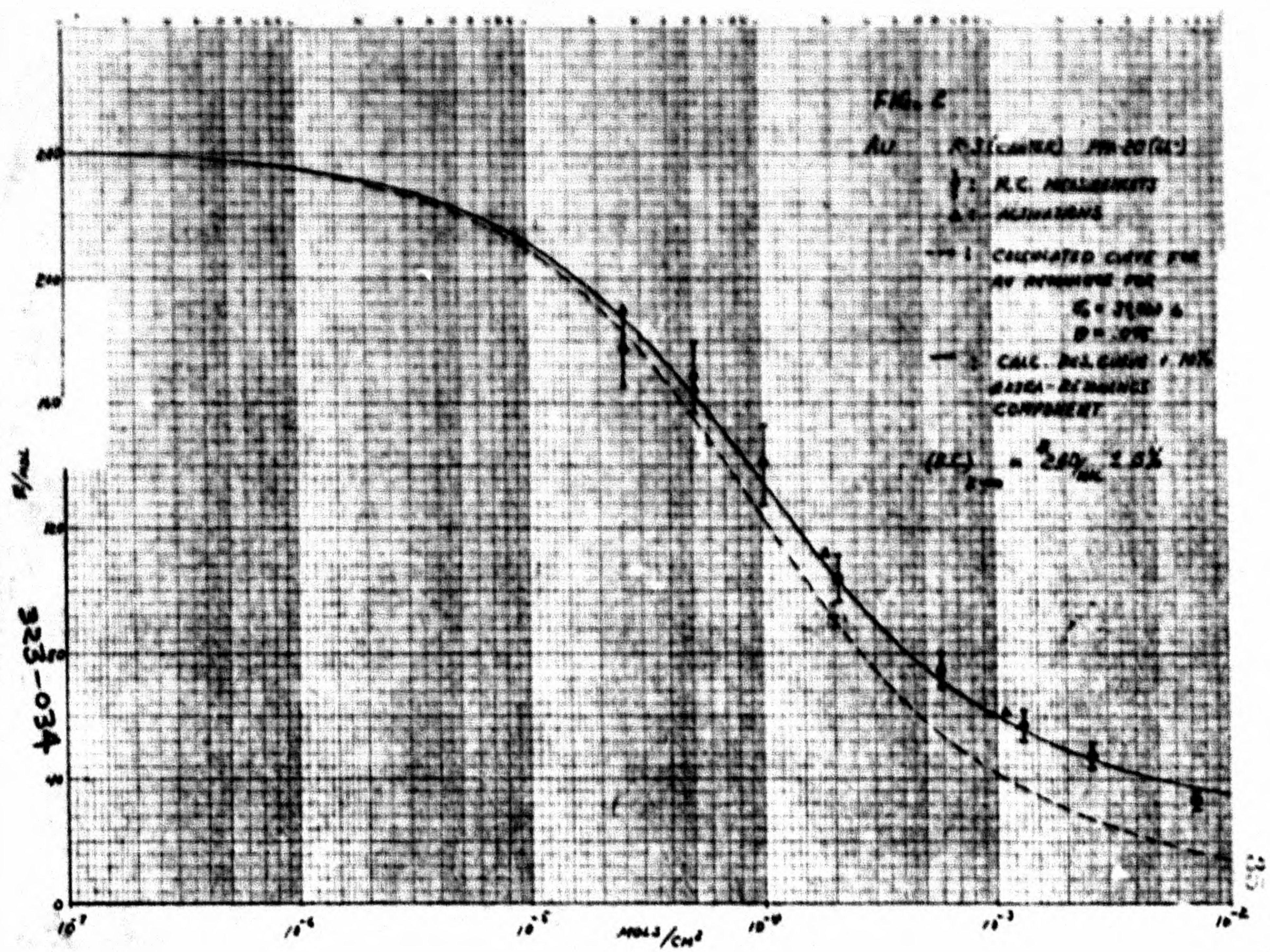
Au
R.C. MEASUREMENTS
CALCULATED CURVE FOR
COMPONENT
MOLS/CM²
323-034

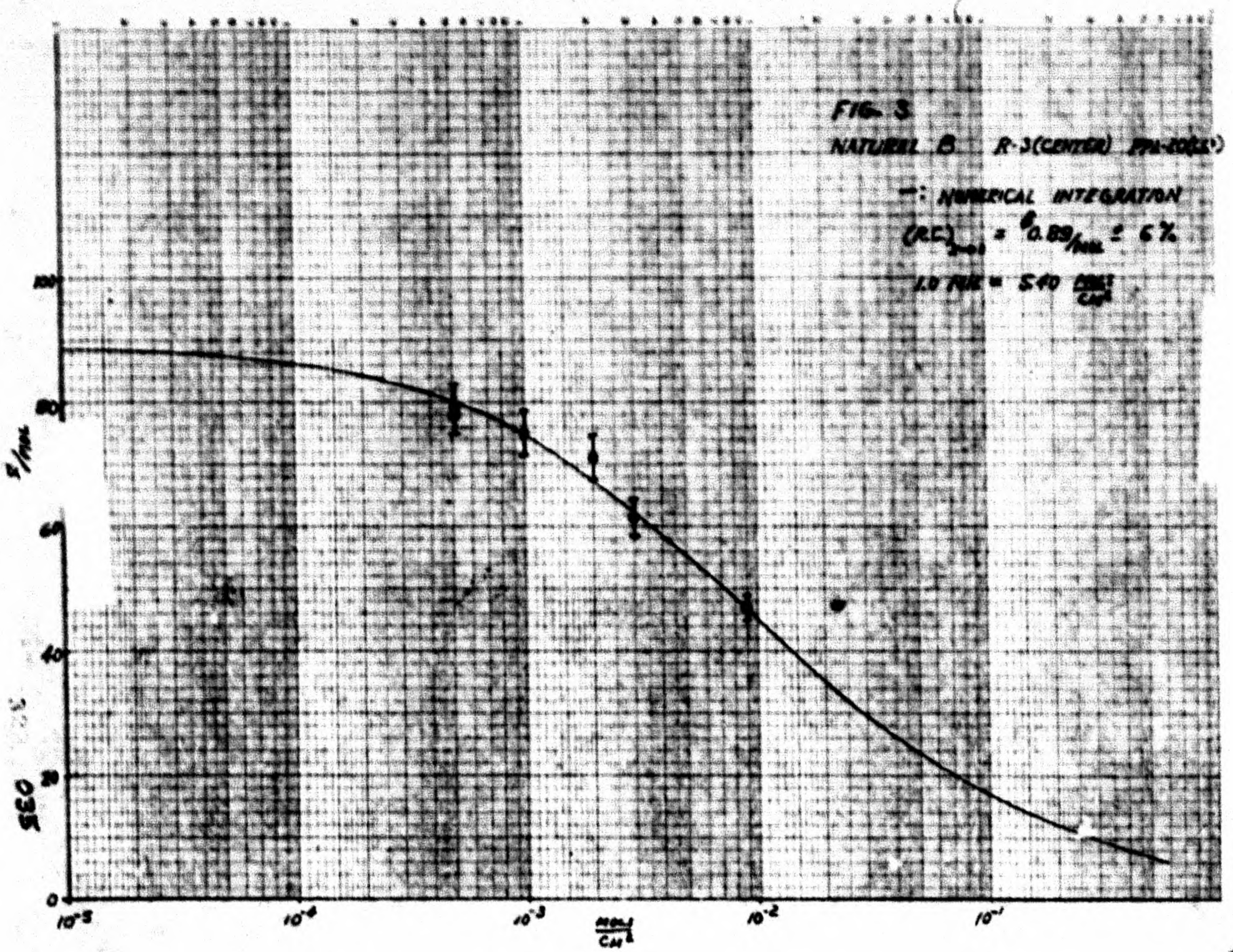
FIG. 3
NATUREL B R-3(CENTER)
NUMERICAL INTEGRATION
± 6%
10⁻⁵
10⁻⁴
10⁻³
10⁻²
10⁻¹
100
80
60
40
20
0

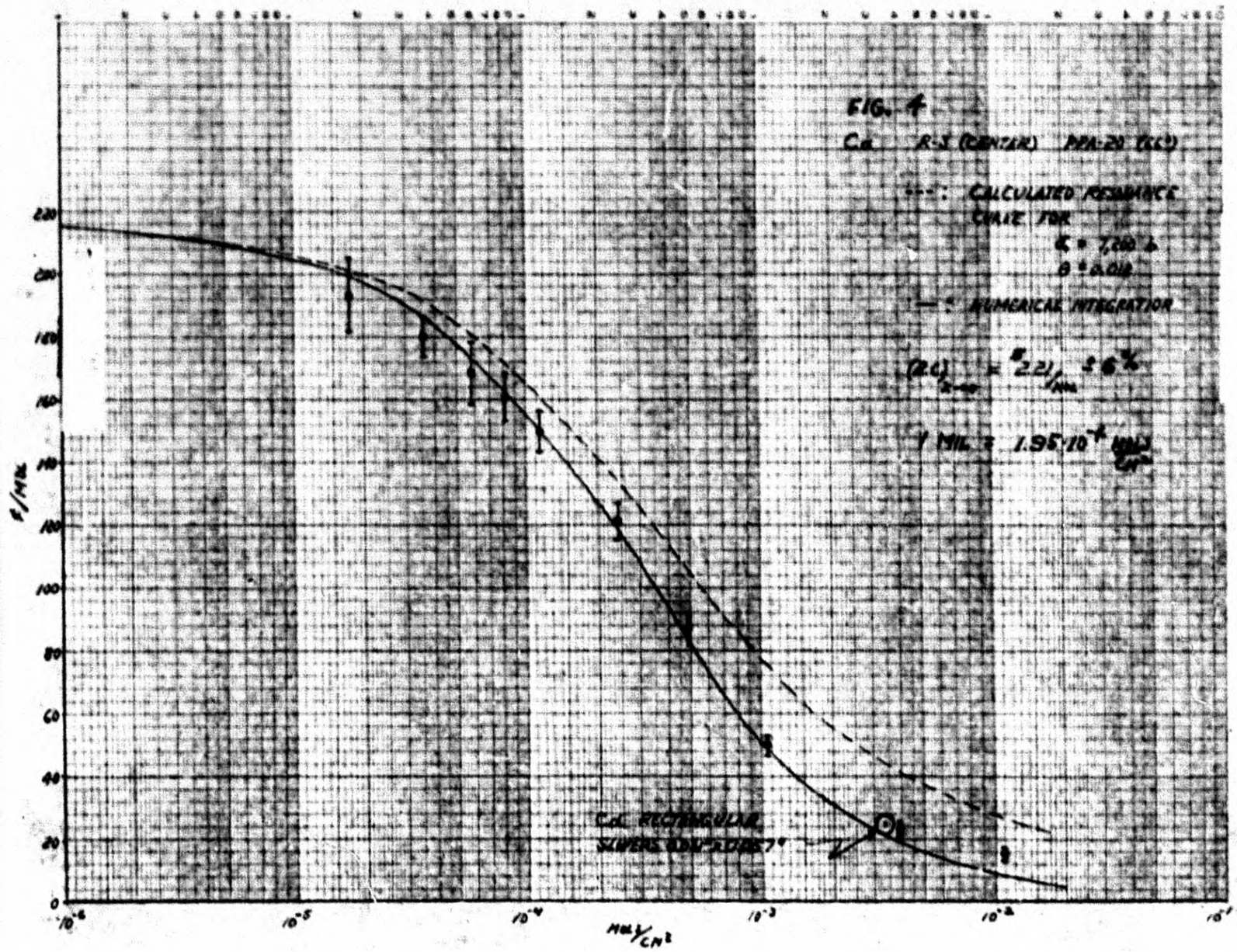
FIG. 4
C.d. R-S (RENZIR) PPA:20 (CC)
---: CALCULATED RESISTANCE CURVE FOR
K = 7,200 Δ
θ ± 0.02
— : NUMERICAL INTEGRATION
$(R_c)_{\theta=0} = \frac{\rho}{2.21 t_{MIL}} \pm 6\%$
1 MIL = $1.95 \cdot 10^{-4}$ inch
C.d. RECTANGULAR SLIVERS CONFIGURATION
Ω/MIL
MIL/CM²
0
20
40
60
80
100
120
140
160
180
200
220
10^{-6}
10^{-5}
10^{-4}
10^{-3}
10^{-2}
10^{-1}

37

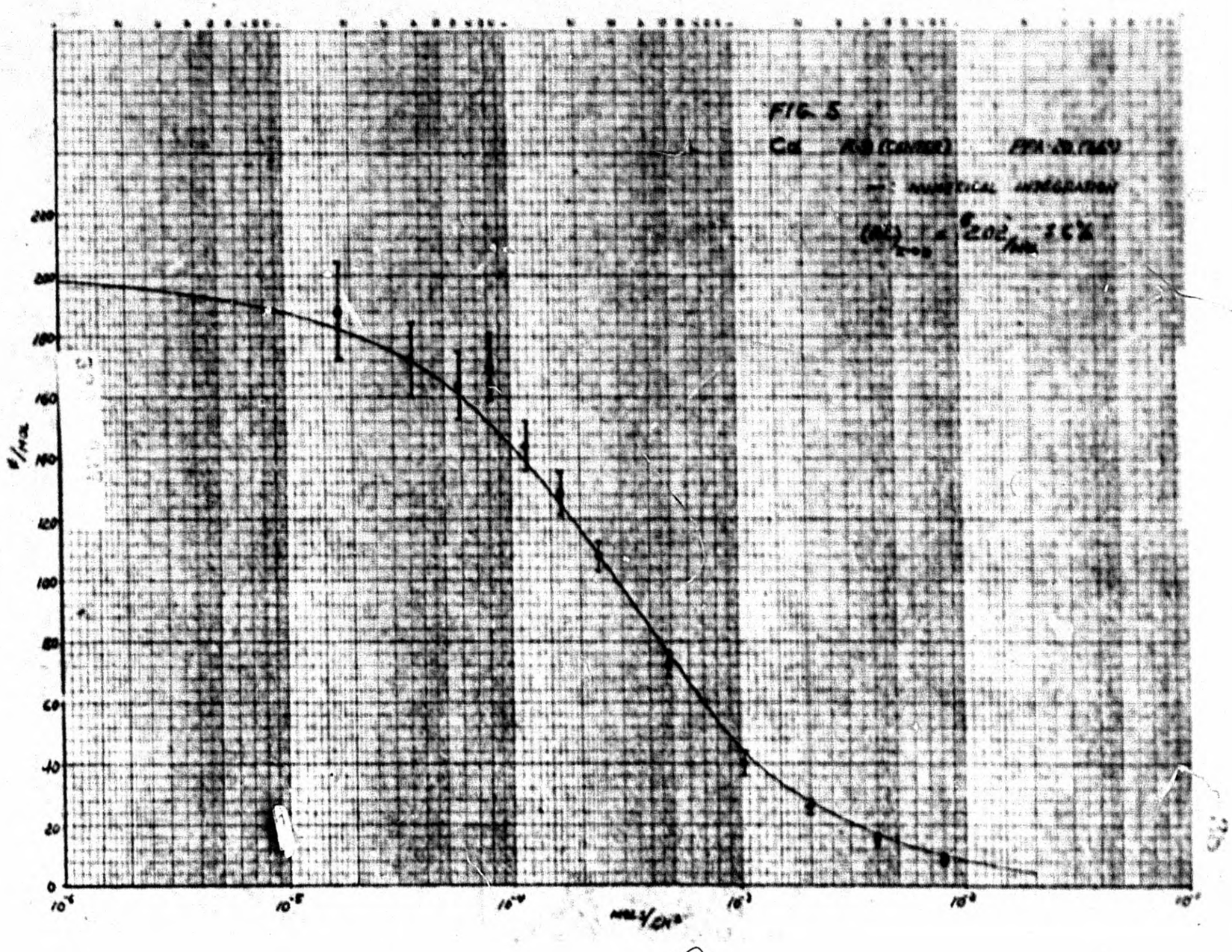
FIG. 5
200
180
160
140
120
100
80
60
40
20
0
10^{-6}
10^{-5}
10^{-4}
10^{-3}
10^{-2}
10^{-1}

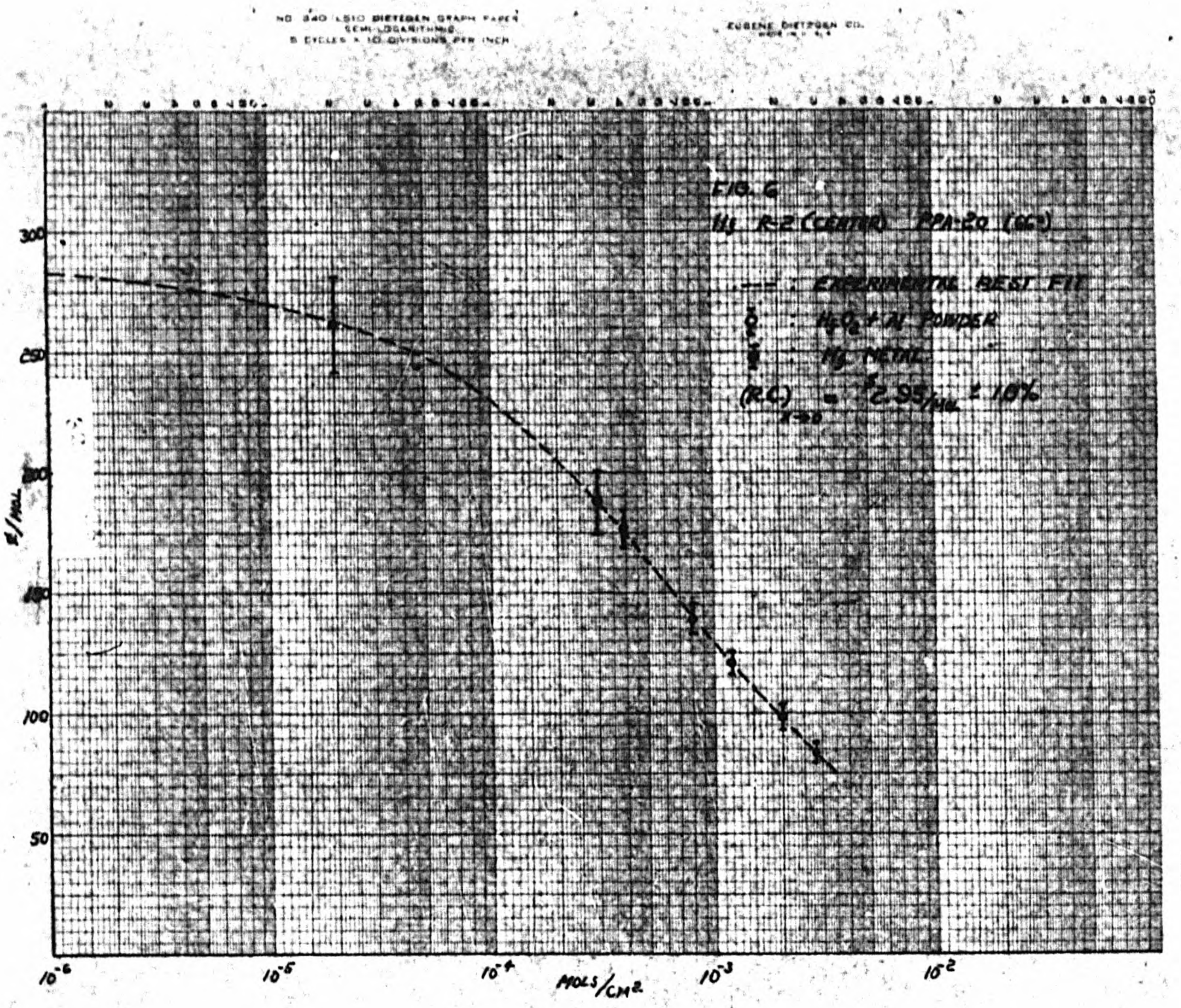
NO. 340 L510 DIETZGEN GRAPH PAPER
SEMI-LOGARITHMIC
5 CYCLES X 10 DIVISIONS PER INCH
EUGENE DIETZGEN CO.
FIG. 6
Hg R-2 (CENTER) PPA-20 (66°)
- - - : EXPERIMENTAL BEST FIT
H2O2 + Al POWDER
Hg METAL
(R.C.) = $2.95/ML ± 10%
300
250
200
150
100
50
¢/MOL
10^-6
10^-5
10^-4
10^-3
10^-2
MOLS/CM2

FIG. 7

R_{th} R-3 (CENTER) PPR-20 (Be)

CALCULATED RESONANCE CURVES

— : σ_c = 6,600 b
Θ = 0.06

— : σ_c = 4,600 b
Θ = 0.03

$(RC)_{R-3}$ = $\$_{LCO}/_{mass}$ ± 20%

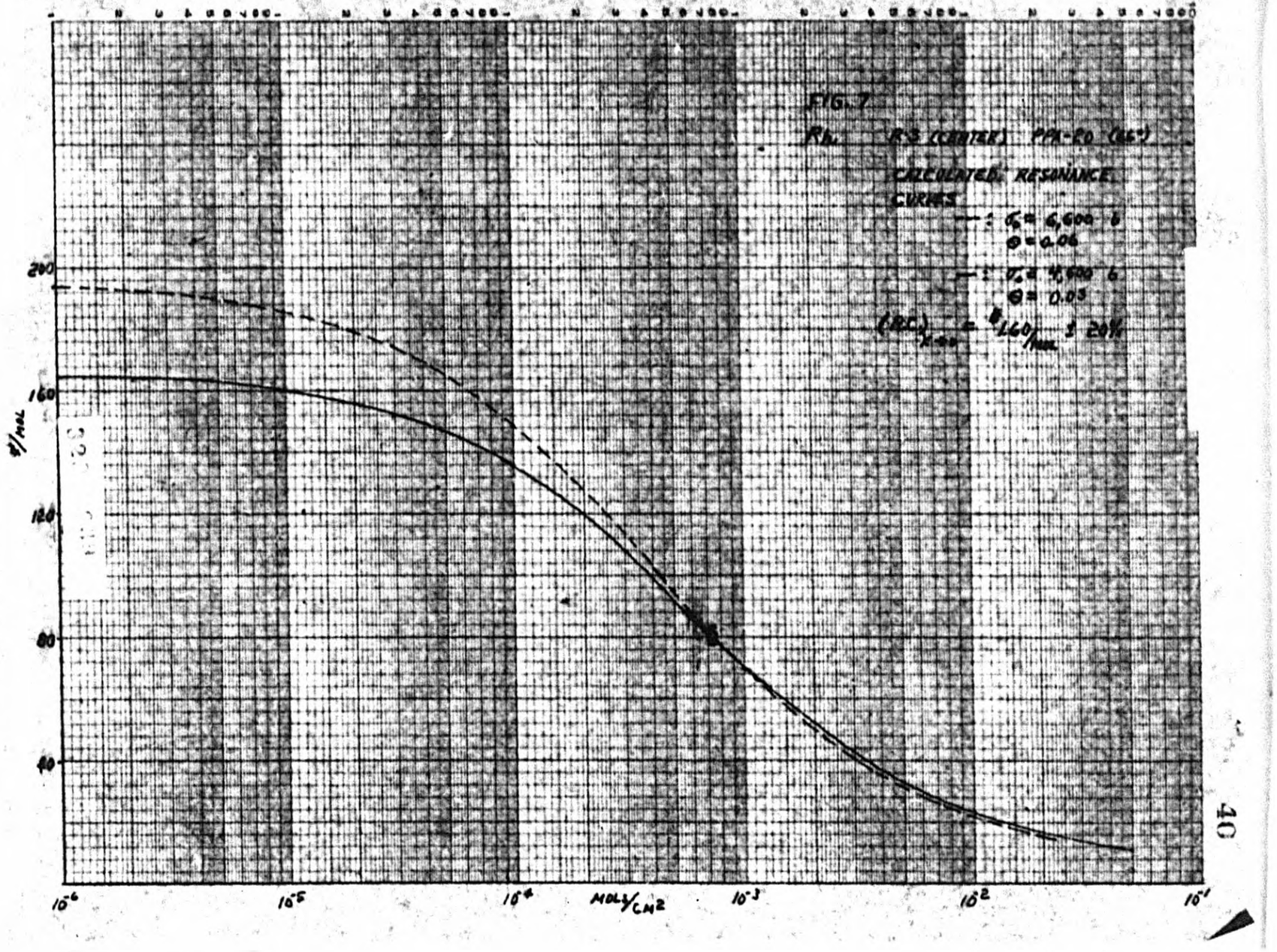

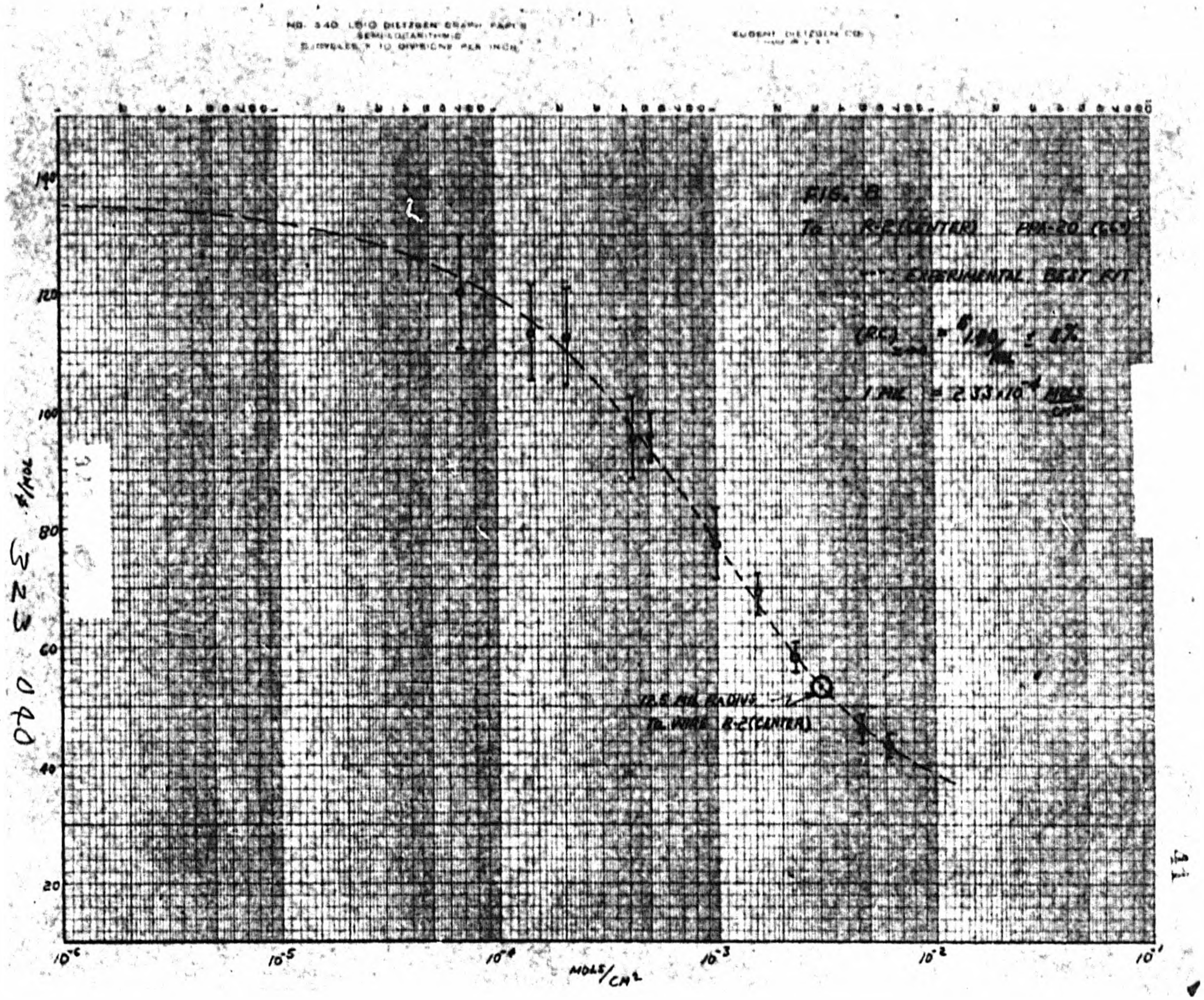
FIG. 8
EXPERIMENTAL BEST FIT
20
40
60
80
100
120
140
10^{-6}
10^{-5}
10^{-4}
10^{-3}
10^{-2}
10^{-1}
MOLS/CM²

323 040

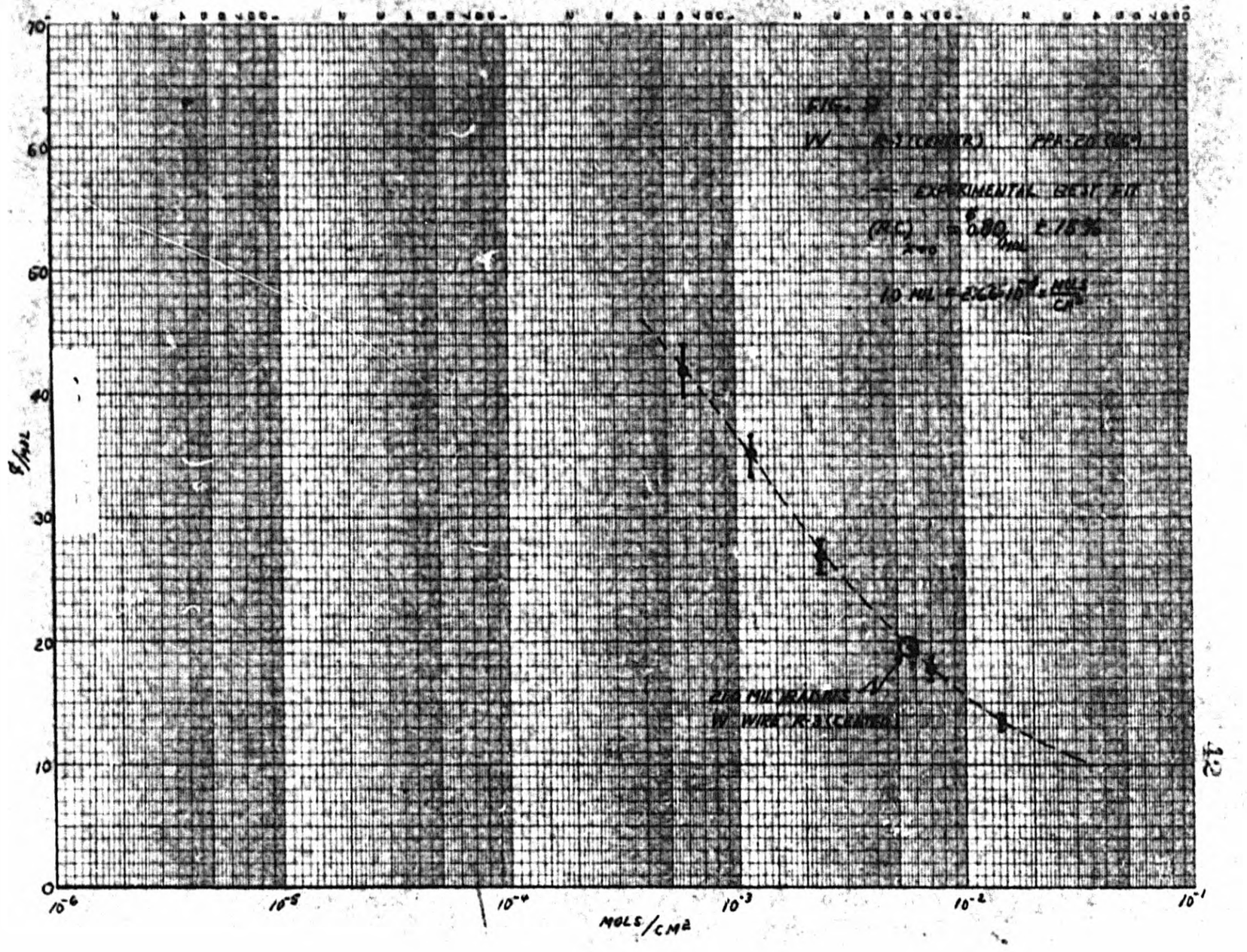

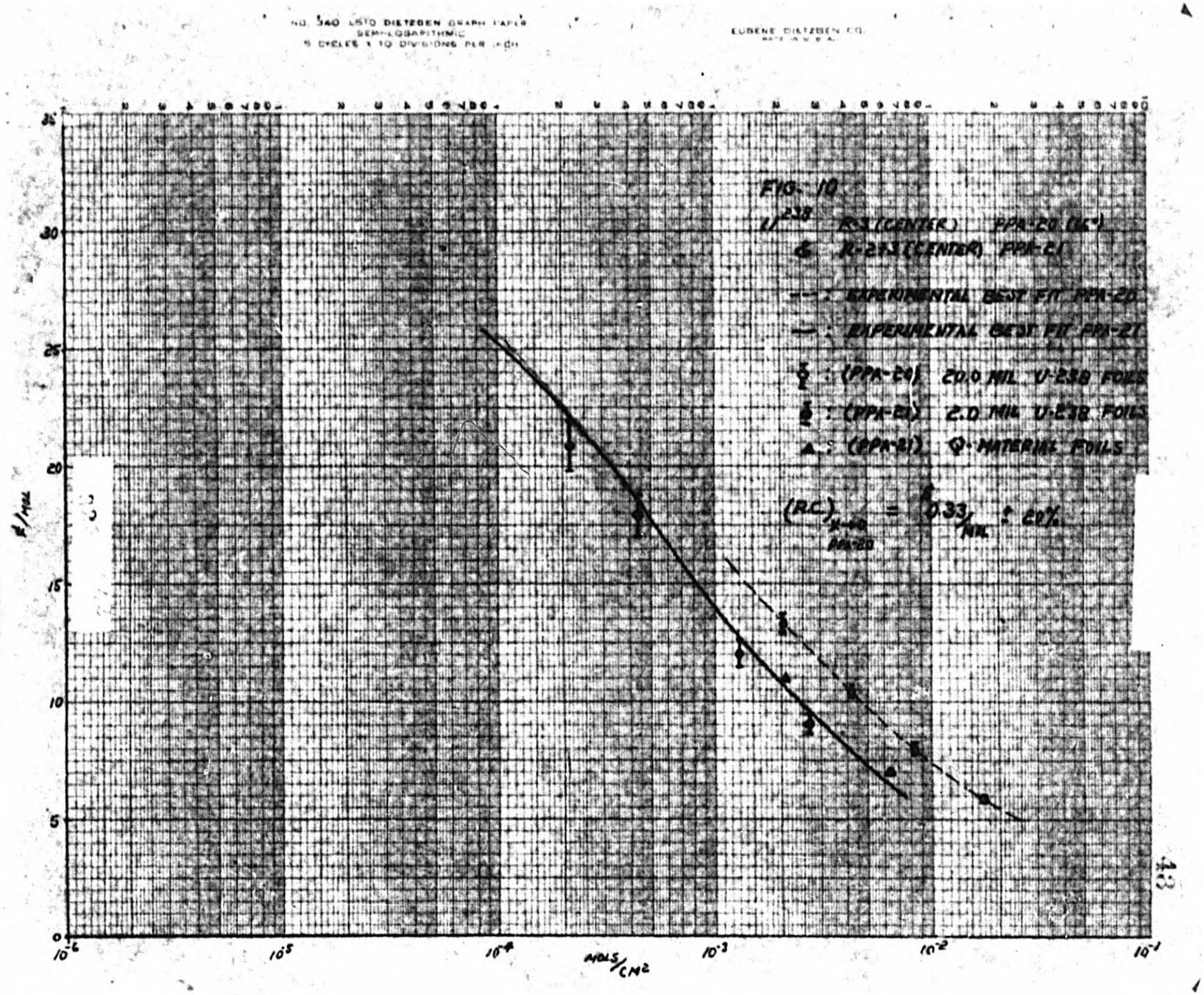
NO. 340 KEUFFEL & ESSER CO. GRAPH PAPER
SEMI-LOGARITHMIC
5 CYCLES X 10 DIVISIONS PER INCH
EUGENE DIETZGEN CO.
FIG- 10
U-238 R-23 (CENTER) FPX-20 (BC)
R-233 (CENTER) FPX-21
---: EXPERIMENTAL BEST FIT FPX-20
—: EXPERIMENTAL BEST FIT FPX-21
(FPX-20) 20.0 MIL U-238 FOILS
(FPX-21) 2.0 MIL U-238 FOILS
(FPX-21) Q-MATERIAL FOILS
(R.C.) = 0.33/MIL ± 20%
R/MIL
0
5
10
15
20
25
30
10^{-6}
10^{-5}
10^{-4}
10^{-3}
10^{-2}
10^{-1}
ABLS/CM²

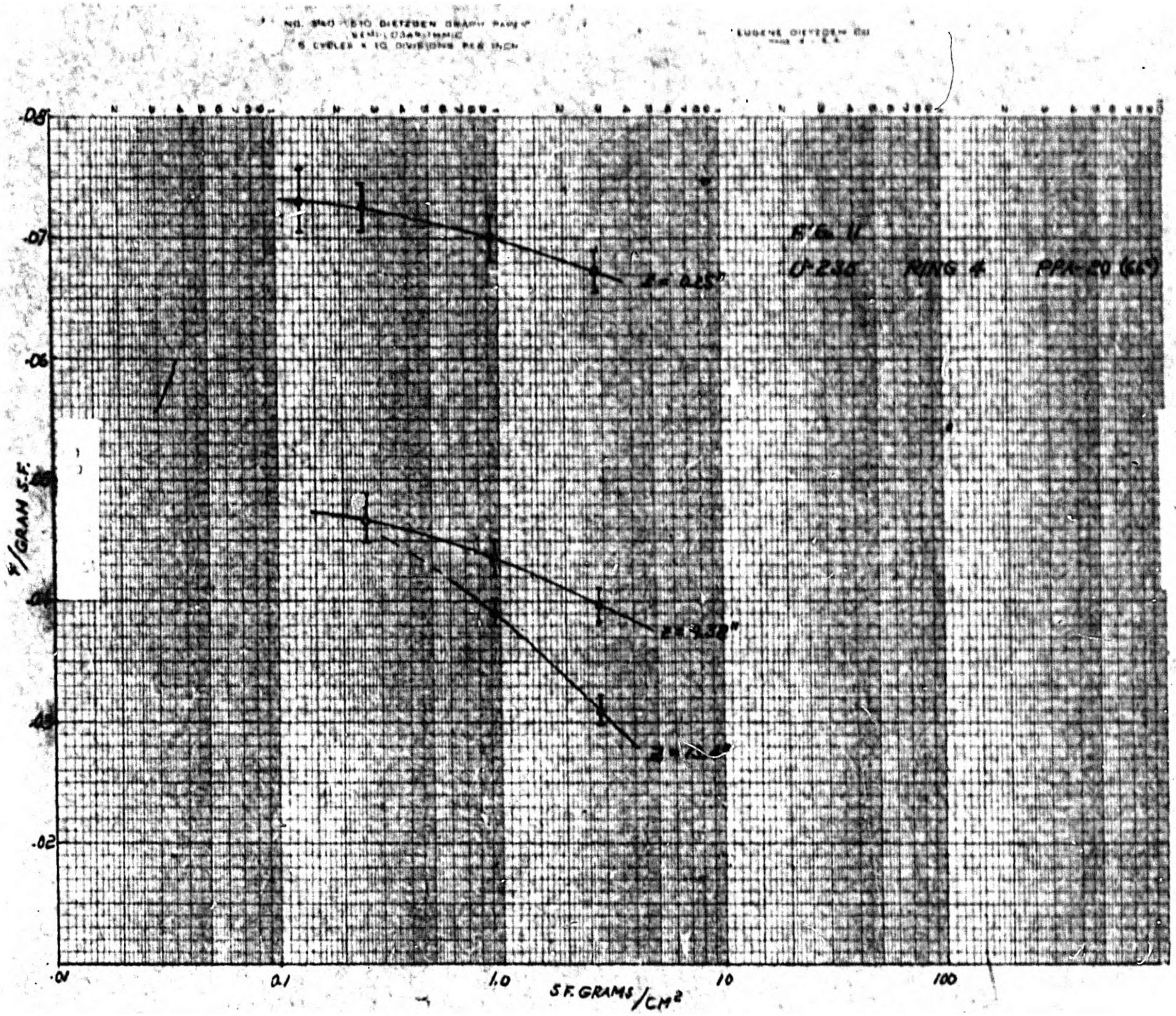

RING 4
PPA-20
.08
.07
.06
.02
.01
0.1
1.0
10
100
S.F. GRAMS/CM²

NO. 340 - LS10 DIETZGEN GRAPH PAPER
SEMI-LOGARITHMIC
5 CYCLES X 10 DIVISIONS PER INCH

EUGENE DIETZGEN CO.
MADE IN U.S.A.

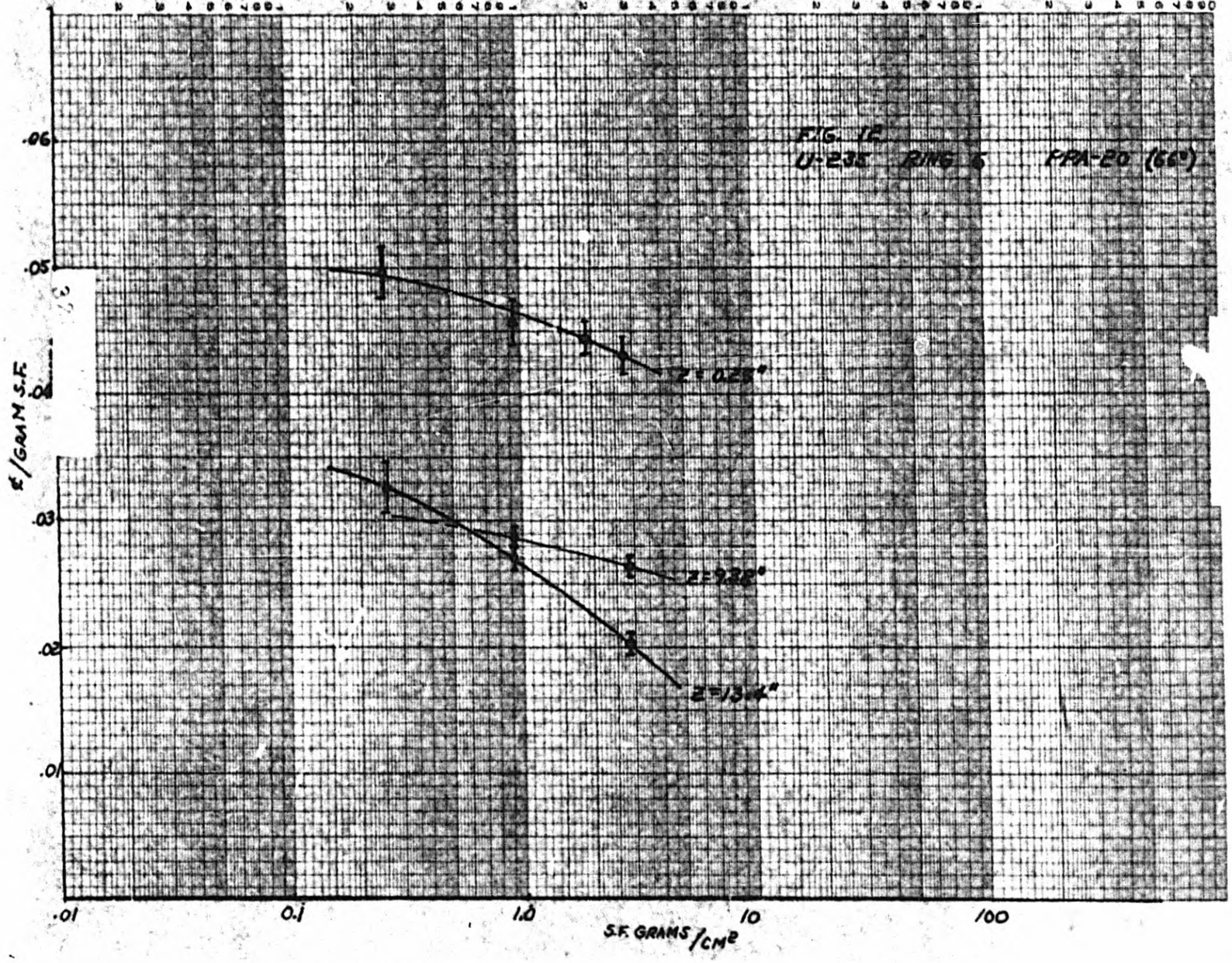

FIG. 12
U-235 RING 6 FFA-20 (66)

NO. 340 L510 DIETZGEN GRAPH PAPER
SEMI-LOGARITHMIC
5 CYCLES X 10 DIVISIONS PER INCH

EUGENE DIETZGEN CO.
MADE IN U.S.A.

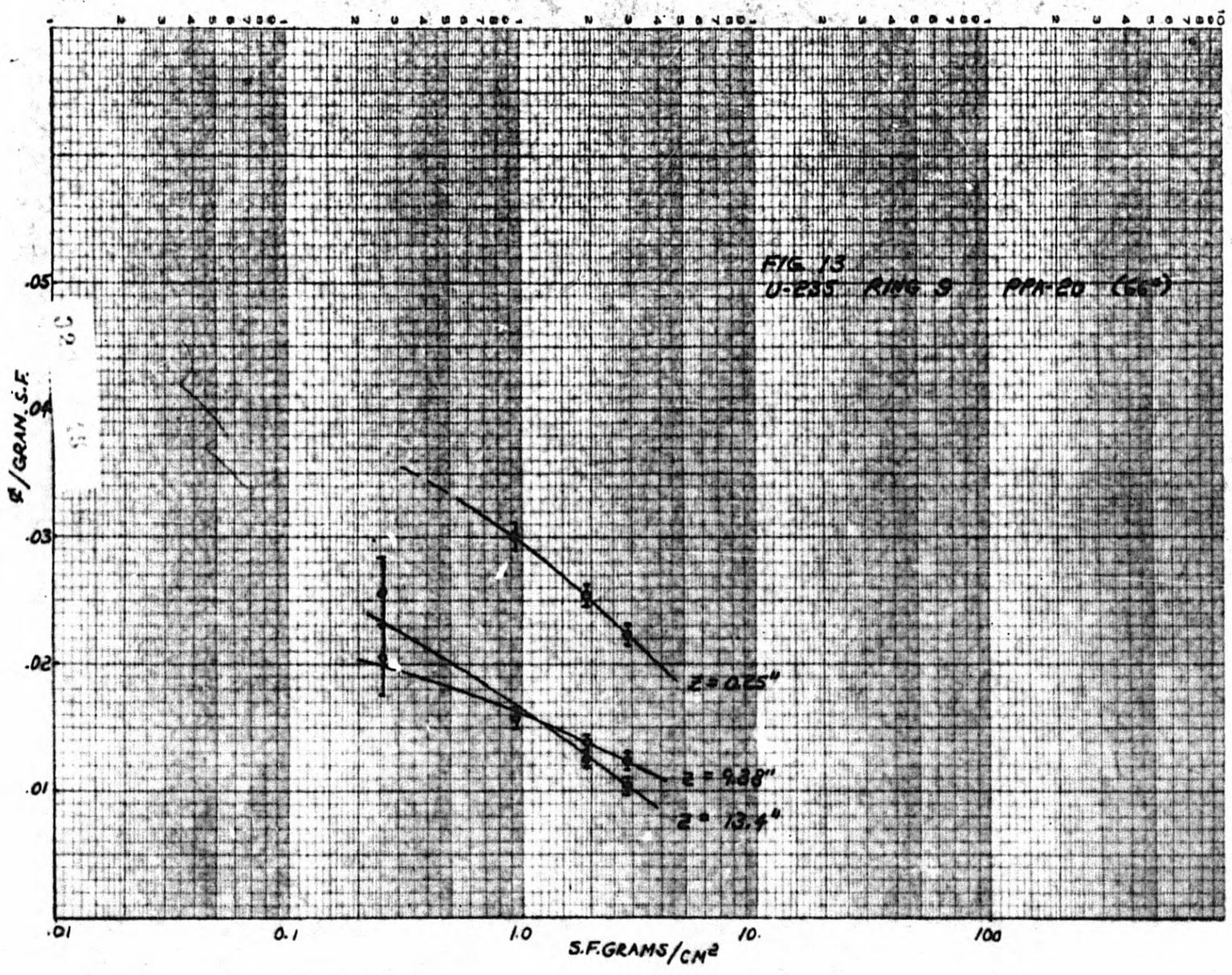

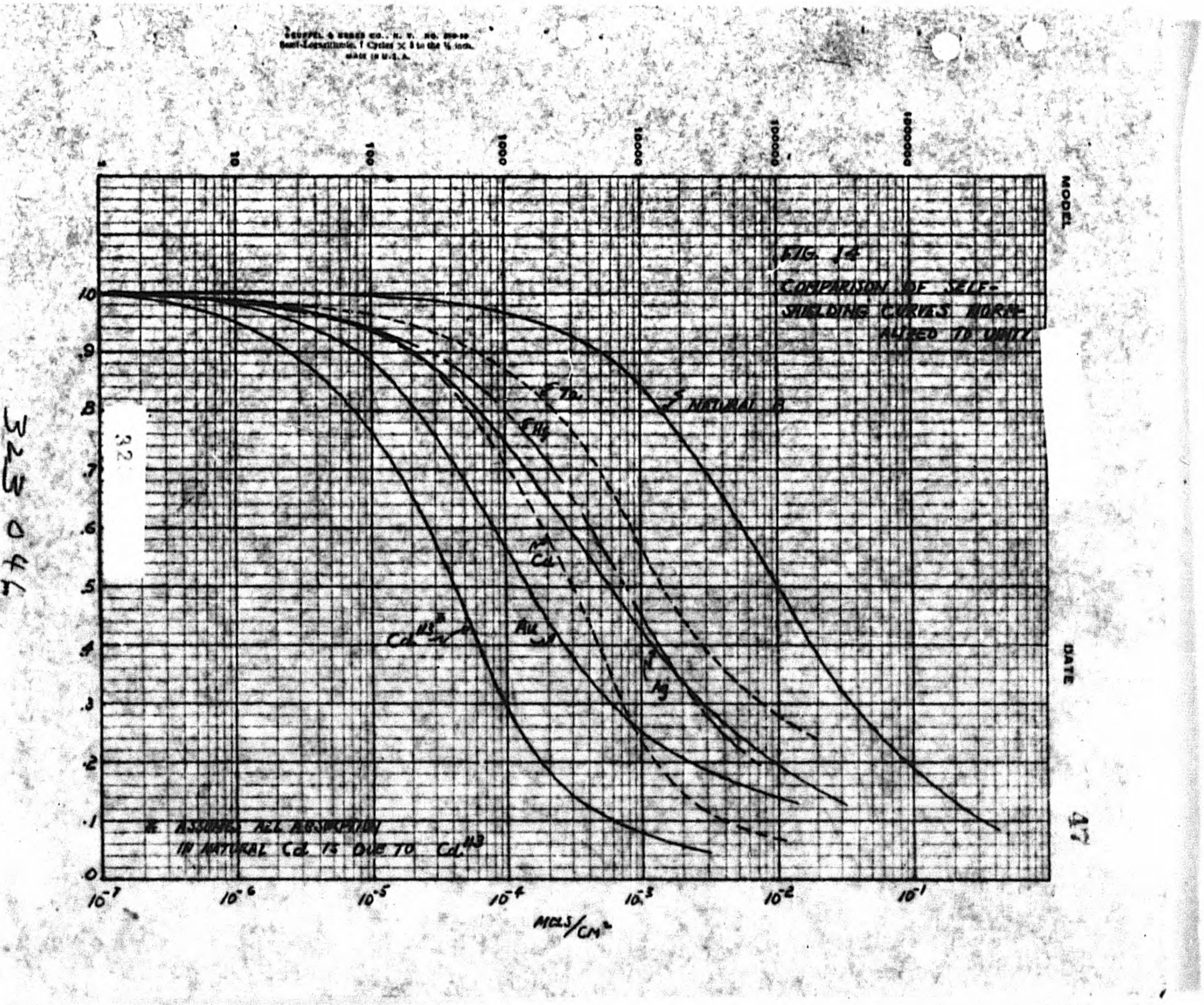

FIG. 14
COMPARISON OF SELF-SHIELDING CURVES NORMALIZED TO UNITY
NATURAL B
Th
Hg
Cd
Cd113*
Au
Hg
* ASSUMES ALL ABSORPTION IN NATURAL Cd IS DUE TO Cd113
1.0
.9
.8
.7
.6
.5
.4
.3
.2
.1
0
10-7
10-6
10-5
10-4
10-3
10-2
10-1
MOLS/CM2

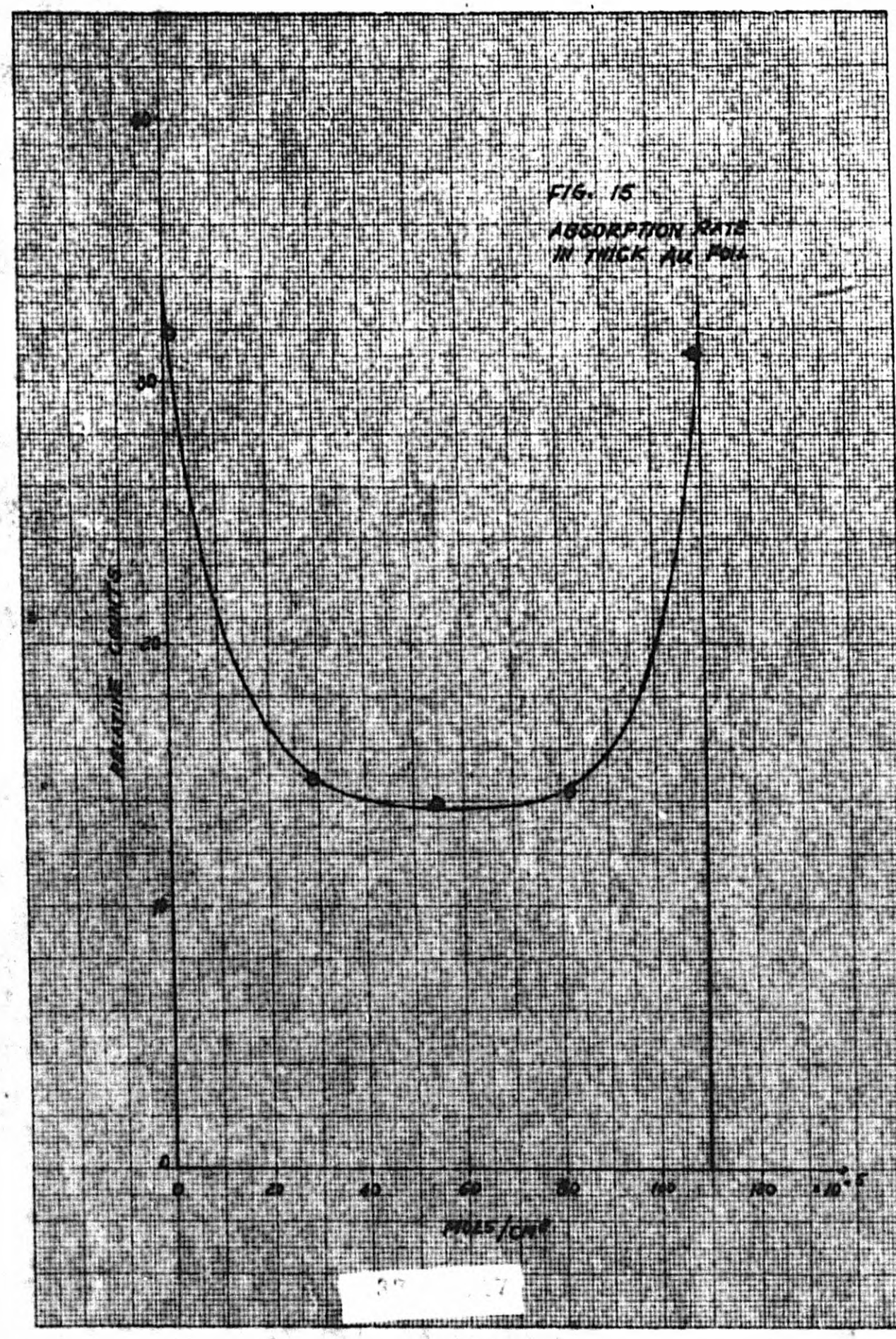

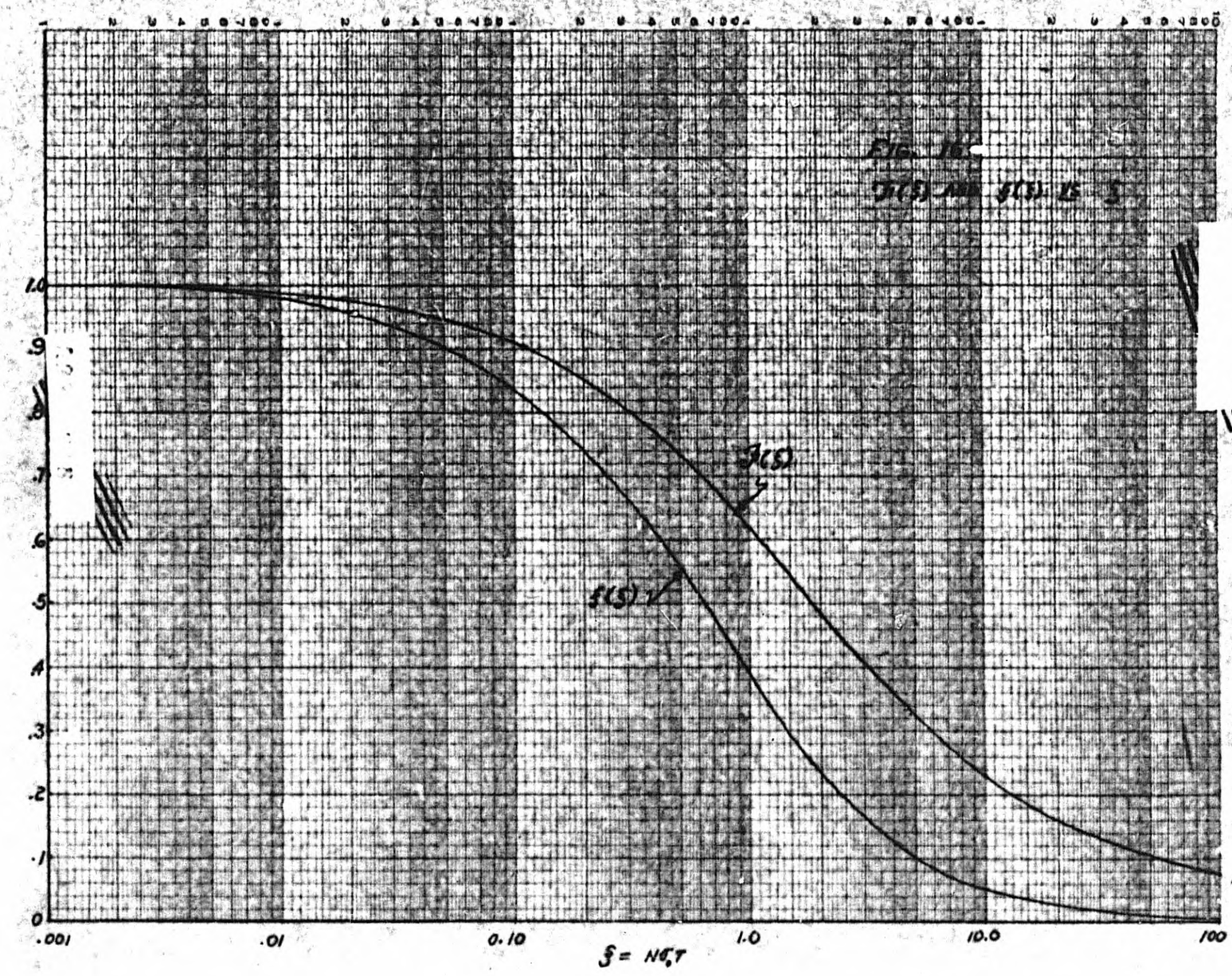

K&E LOGARITHMIC 359-125G
KEUFFEL & ESSER CO.

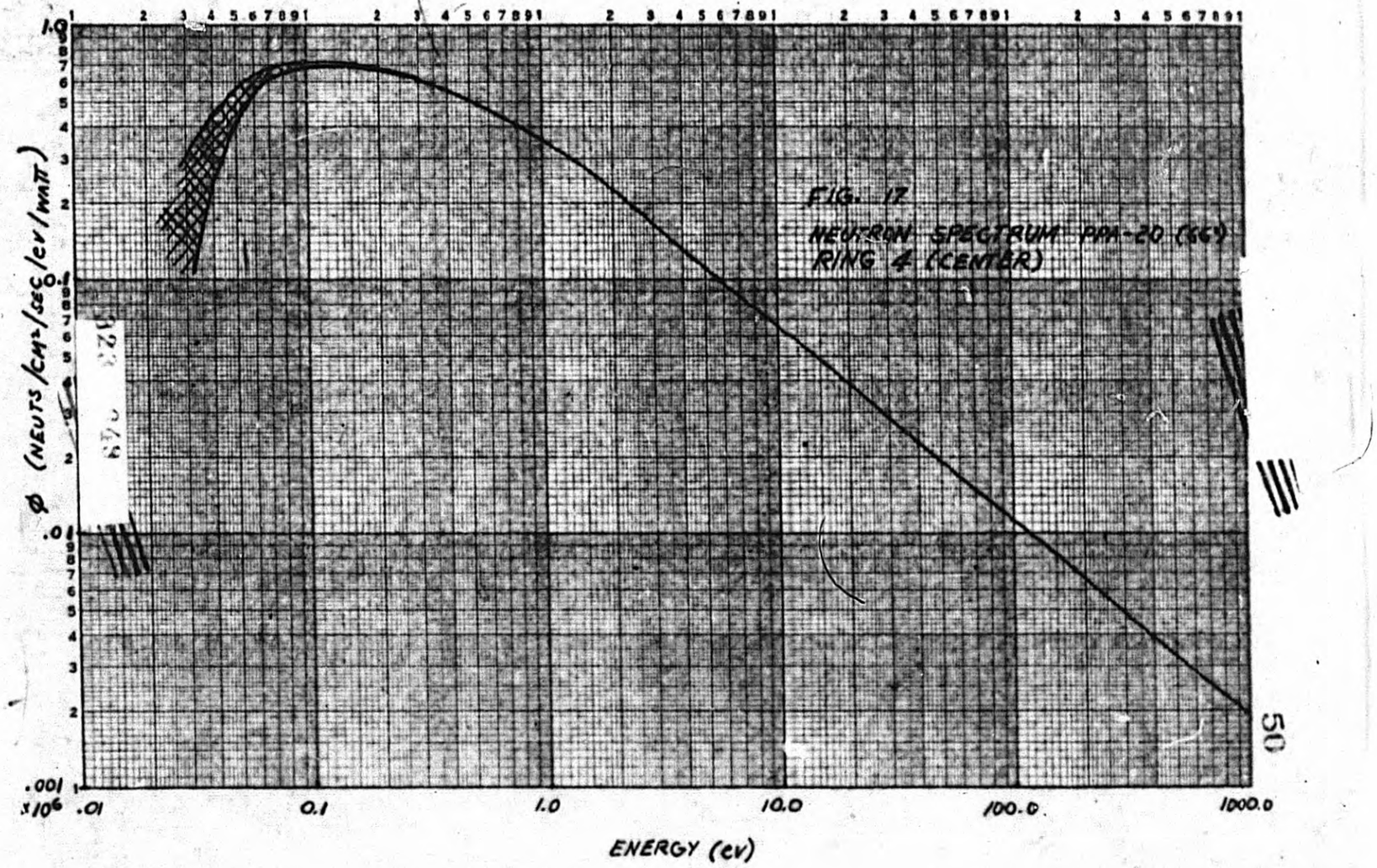

FIG. 17
NEUTRON SPECTRUM PRM-20 (SGC)
RING 4 (CENTER)

50

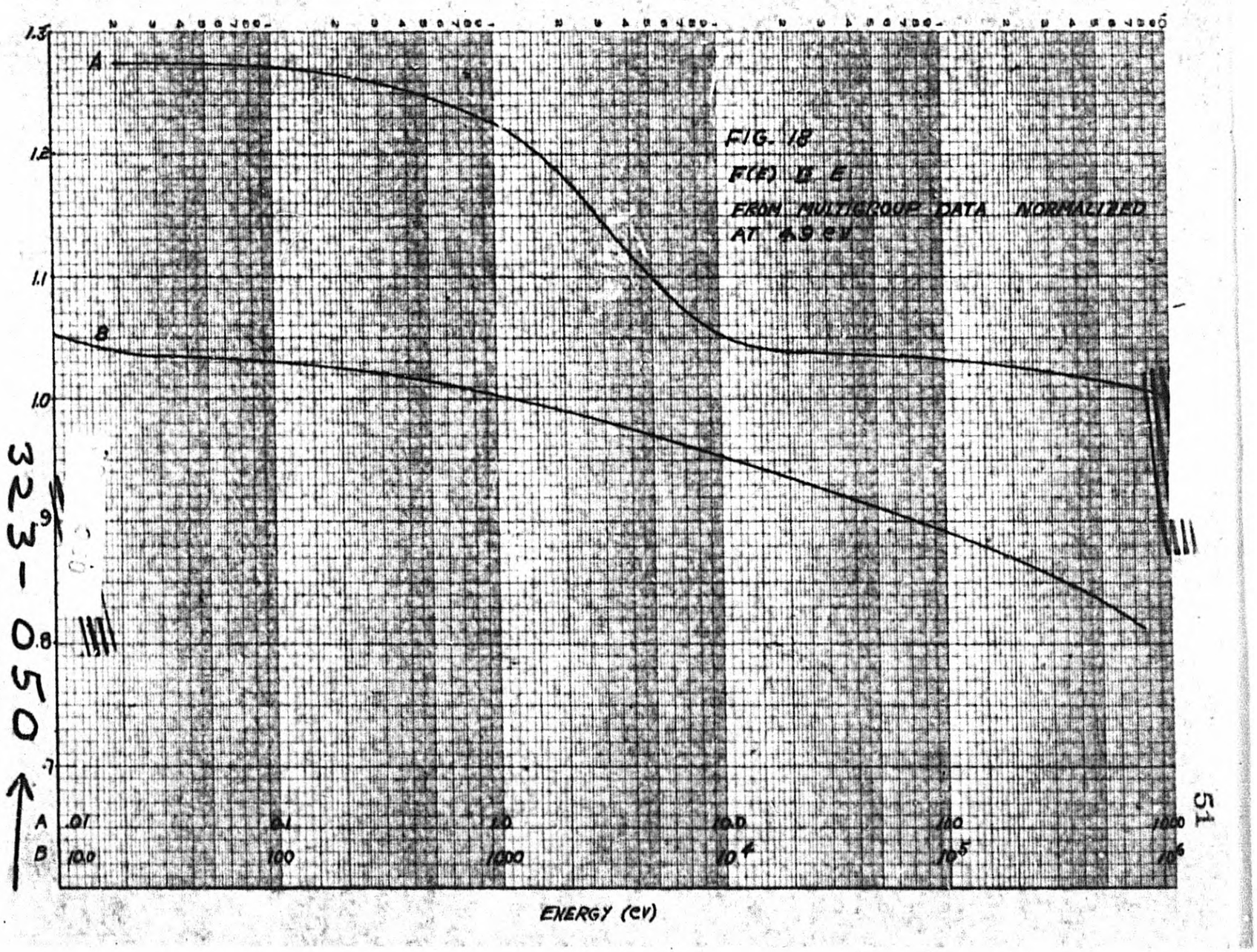

FIG. 18
F(E) ≡ E
FROM MULTIGROUP DATA NORMALIZED AT 4.9 eV

323-050

END